ADVANCED MECHANICS AND COMPOSITES TECHNOLOGY LAB
OREGON STATE UNIVERSITY

Calibration Methods for an Aerolab 375 Sting Balance to be used in Wind Tunnel Testing

Sean E. Van Hatten

17 May, 2013

Internal force, or sting, balances are used in wind tunnel testing to measure the total force and moment imposed on an aerodynamic structure. A sting balance operates through strain gauges converting strain from externally applied loads to voltage signals. An accurate measuring device is of paramount importance in wind tunnel testing, and this thesis concerns itself with calibrating such measurement device for use with micro air vehicles in a wind tunnel. A calibration matrix was found to convert the voltage output of the balance to force and moment data. Known loads were applied to the different channels of the sting balance and a custom made program was used to read and post process the voltages produced by the strain gauges in the balance under load. A relationship between voltage and load was then found and used to produce the calibration matrix. The calibration matrix was then inputted into a different program to test the accuracy and resolution of the balance by applying known loads, as a reference, and comparing the measured forces to the reference.

Important Calibration Data

The calibration matrix for the Aerolab 375 sting balance used in the Advanced Mechanics and Composites Technology lab at Oregon State University was found to be

-68725.362	70572.741	-608.535	-5832.989	-24308.328	133.062
-7278.844	583447.882	17524.047	19019.789	-271621.758	-10315.883
358.179	-85569.646	-237901.044	-2826.249	38309.891	120287.584
1.581	-1592.123	-245.894	-5254.389	511.840	-649.803
569.752	-43657.544	-1251.340	-1171.897	18277.205	756.145
4.760	-1182.746	-3797.157	-33.443	535.714	1556.625

Calibration Matrix Fig. 1

to within an approximate error of (see Chapter 4 for a more in depth discussion of the accuracy)

F_x	.604 %
F_y	1.662 %
F_z	.904 %
M_x	4.369 %
M_y	12.368 %
M_z	16.414 %

Average percentage error of each channel Fig. 2

and standard deviation of

F_x	+/- .065 N
F_y	+/- .062 N
F_z	+/- .067 N
M_x	+/- .499 Ncm
M_y	+/- .509 Ncm
M_z	+/- .568 Ncm

Chart of channel standard deviations Fig. 3

and finally with a 95% confidence, the average confidence intervals are

F_x	+/- .020 N
F_y	+/- .020 N
F_z	+/- .022 N
M_x	+/- .166 Ncm
M_y	+/- .157 Ncm
M_z	+/- .179 Ncm

Average confidence intervals for each channel with 95% confidence Fig. 4

Table of Contents

1. Introduction

1.1 Motivation

Wind tunnel testing is a great resource for aerodynamic design as it allows measurements to be performed in a controlled environment on a model. In wind tunnel testing, there are three main forces acting on a body which are lift, weight, and drag. Along with these forces, there are also associated moments namely rolling, yawing, and pitching moment (see Fig. 1.1).

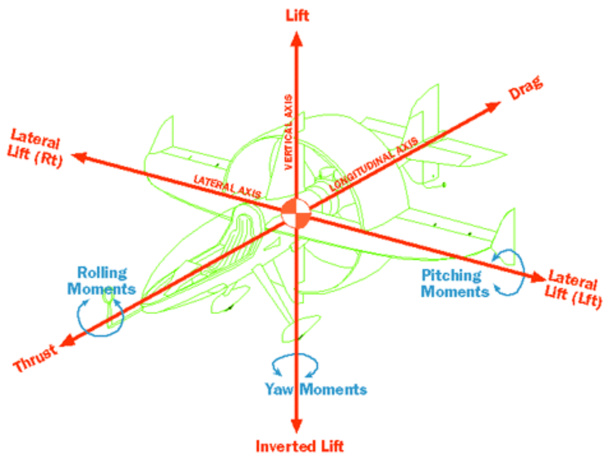

The aerodynamic forces and moments on a model[7] Fig. 1.1

Micro air vehicles (MAVs) are the primary focus for wind tunnel testing at Oregon State University (for an excellent paper on one of the first MAVs, see AeroVironment's paper on the Black Widow[11]). Most aircraft are controlled by hinged surfaces attached to the stabilizers and wings; however, by drawing inspiration from nature, the focus of this research is on wing morphing technology. Instead of the wings being solid surfaces, their shape can be changed to alter the flight characteristics of the aircraft (Fig. 1.2).[1] Before attempting to fly these aircraft, their flight characteristics can be analyzed in a wind tunnel.

MAV with wing morphing capability [1] Fig. 1.2

Another area of research in MAVs is associated with multiple rotor aircraft (Fig. 1.3). These aircraft use three or more motors and rotors to provide lift and control. These aircraft are significantly stable and highly maneuverable; two attributes which are somewhat conflicting characteristics. Rotors for these aircraft are critical since they are required for both lift and control, and they must operate correctly in many different flight regimens. It is important to understand the characteristics of these rotors in static as well as dynamic conditions, so Oregon State is currently performing wind tunnel testing on these micro rotors.

Multi-rotor air vehicle [2] Fig 1.3

For wind tunnel testing to be effective, clear and precise measurements of these forces and moments are required. Internal force balances are commonly used to make these measurements. A sting is the apparatus that holds a model in a wind tunnel (Fig. 1.4). The internal force balance houses a series of strain gauges inside the sting, turning the sting into a measuring device. Because of this, the internal force balance is often referred to as a sting balance. The goal of this project is the calibration of the sting balance by obtaining a calibration matrix and certifying the performance of the balance.

A sting balance in use [12] Fig. 1.4

1.2 Sting Balance

Measurements are accomplished by the use of strain gauges inside the balance. The electrical resistance of a strain gauge changes as it is stretched or contracted. If a constant current is applied to the gauge, the voltage will change via Ohm's law.

$$\Delta V = I \Delta R \qquad \text{Eq. 1.1}$$

This is the basic operating principal behind the balance. One strain gauge is used for each component of the balance with one, so they stretch and compress according to the externally applied loads (Fig. 1.5). A six component sting balance is used which gives six voltages which correspond to five forces and one moment: normal 1 and 2 (N1 and N2), side one and two (S1 and S2), and axial (A) forces and the rolling (R) moment. Since N1 and N2, and S1 and S2, are located at different points on the balance, the forces can be solved, through the calibration matrix, to find the two missing moments; the pitching and yawing moment. After the moments have been solved for, the more traditional aerodynamic forces and moments can be discussed. These forces and moments are referred to as the axial force (AF), side force (SF), normal force (NF), rolling moment (RM), yawing moment (YM), and pitching moment (PM) respectively (Fig. 2.1). The main purpose of the calibration is to convert the voltage output of the strain gauges to meaningful force and moment data.

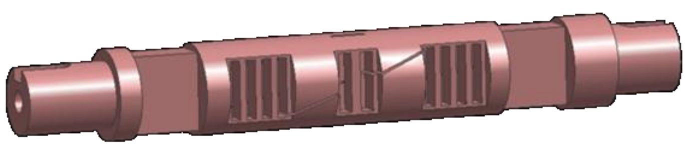

CAD model of a typical sting balance [8] Fig. 1.5

Ideally, the balance is constructed in a way that there are no interactions between components, but realistically this is impossible. When a load is applied in a pure direction, for instance F_x, the 5 other components will develop output voltages as well. The other purpose of calibrating a sting balance is to compensate for these interactions. For the purposes of this particular balance, only first order interactions will be considered. That is, the output of the other five components when one component is loaded. Second order interactions would be the response of 4 components when two components are loaded. The same idea can be applied to higher order interactions.

The sting balance available in the lab is the Aerolab 375. Wind tunnel testing of MAVs and small rotors generates small loads, so the primary concern when choosing a sting balance for this type of testing is high resolution at loads on the order of 1-5N. Table 2.1 shows the maximum loads of the Aerolab 375 sting balance:

NF	44.5 N
SF	44.5 N
AF	17.8 N
PM	169.5 Ncm
SF	169.5 Ncm
RM	564.9 Ncm

Maximum Loads of the Aerolab 375 sting balance[3] Table 1.1

1.3 Theory

Raw data from the sting balance can be represented as a 1x6 matrix of voltages.

$$\begin{bmatrix} V_1 & V_2 & V_3 & V_4 & V_5 & V_6 \end{bmatrix}$$

Voltage matrix Eq. 1.2

Likewise, the pertinent data can be represented as a 6x1 matrix of forces and moments.

$$\begin{bmatrix} F_x & F_y & F_z & M_x & M_y & M_z \end{bmatrix}^T$$

Load matrix Eq. 1.3

When only concerned with first order interactions, raw data can be translated to meaningful measurements via a 6x6 calibration matrix.

$$\begin{bmatrix} V_1 & V_2 & V_3 & V_4 & V_5 & V_6 \end{bmatrix} \begin{bmatrix} m_{1,1} & m_{1,2} & m_{1,3} & m_{1,4} & m_{1,5} & m_{1,6} \\ m_{2,1} & m_{2,2} & m_{2,3} & m_{2,4} & m_{2,5} & m_{2,6} \\ m_{3,1} & m_{3,2} & m_{3,3} & m_{3,4} & m_{3,5} & m_{3,6} \\ m_{4,1} & m_{4,2} & m_{4,3} & m_{4,4} & m_{4,5} & m_{4,6} \\ m_{5,1} & m_{5,2} & m_{5,3} & m_{5,4} & m_{5,5} & m_{5,6} \\ m_{6,1} & m_{6,2} & m_{6,3} & m_{6,4} & m_{6,5} & m_{6,6} \end{bmatrix} = \begin{bmatrix} F_x \\ F_y \\ F_z \\ M_x \\ My \\ M_z \end{bmatrix}$$

Voltage to load equation Eq. 1.4

Determining the entries for this matrix requires placing a pure load for each component of the balance and observing the output voltages. By applying a series of loads from low force to high force, slopes for each component can be determined for a specific load condition (See Fig. 1.7 for sample data).

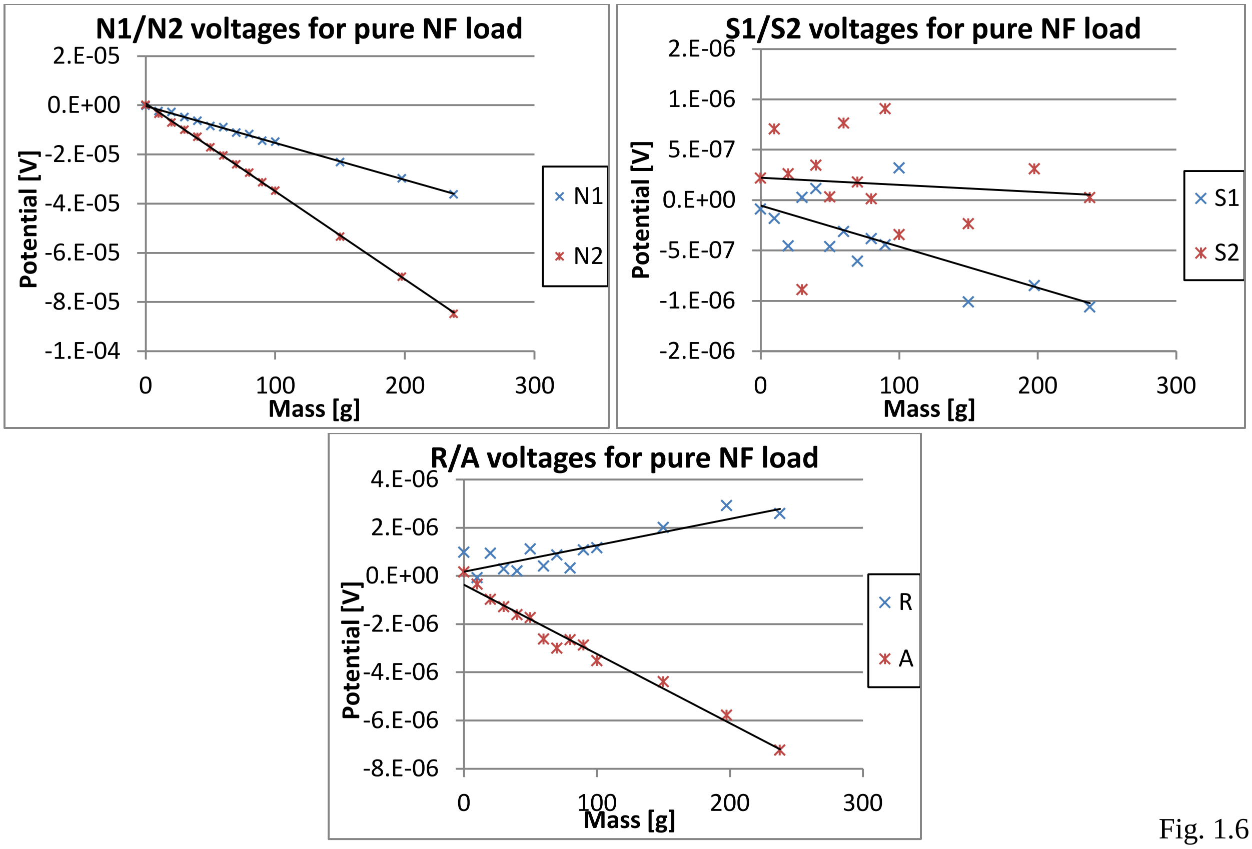

Fig. 1.6

Sample data for a pure N1/N2 load.

For the sample case in Fig. 1.6, the normal direction was loaded with a pure force (0 moment). N1 and N2 show a strong signal as they are the strain gauges that are being loaded. S1 and S2 are not being loaded, so the signal displayed is simply noise. Even though the rolling moment and axial force were not loaded, there is a significant signal; this is an interaction between channels.

Graphs like the ones in Fig. 1.6 are generated for the other pure loading conditions, and the slopes are used to populate a 6x6 matrix. The calibration matrix can be calculated via the following equation (see Appendix 1 for the derivation).

$$\left(\begin{bmatrix} m_{D,A} & m_{D,N1} & m_{D,S1} & m_{D,R} & m_{D,N2} & m_{D,S2} \\ m_{L,A} & m_{L,N1} & m_{L,S1} & m_{L,R} & m_{L,N2} & m_{L,S2} \\ m_{S,A} & m_{S,N1} & m_{S,S1} & m_{S,R} & m_{S,N2} & m_{S,S2} \\ m_{R,A} & m_{R,N1} & m_{R,S1} & m_{R,R} & m_{R,N2} & m_{R,S2} \\ m_{P,A} & m_{P,N1} & m_{P,S1} & m_{P,R} & m_{P,N2} & m_{P,S2} \\ m_{Y,A} & m_{Y,N1} & m_{Y,S1} & m_{Y,R} & m_{Y,N2} & m_{Y,S2} \end{bmatrix}^{-1}\right)^{T} \qquad \text{Eq. 1.5}$$

Calibration matrix equation. m refers to a slope where the first index is the pure load that was imposed and the second index is a balance channel.

Essentially, this matrix equation is the equivalent of taking one slope and inverting it to find the reverse relationship between the voltage and the force, and then transposed to preserve the units.

2. Methods

Calibrating the Aerolab Sting Balance was a 3 step process. First, data for known loads was gathered. This data was then processed to provide some relationship between the voltages given by the balance and the load on the balance, and a matrix was produced from this data. Finally the matrix was used with the balance and known loads to test the accuracy of the system.

The materials and tools required to accomplish this are the Aerolab 375 sting balance, a computer with LabView and the appropriate visual interfaces (VIs) installed, a LabView cRIO (compact reconfigurable input/output) with a wheatstone bridge module and an AID converter modules to run the sting balance, a digital level, a set of masses ranging from 10g to 250g in 10 gram increments up to 100g and then 50g increments thereafter, a vice with 2 axis angle adjustment, and jigs to hang the masses and load the moment channels.

Before any work can be done, the balance needs to warm up for at least 15 minutes to allow the strain gauges and internal electronics to stabilize[3]. The balance has six channels N1, N2, S1, S2, R, and A. These channels are used to calculate the forces and moments used F_x, F_y, F_z, M_x, M_y, M_z (see Fig. 2.1).

Balance with forces and moments labeled Fig. 2.1

To determine the calibration matrix, a relationship between the voltages given by the balance and the known loads needs to be established. The balance needs to be oriented in a way such that the load is only affecting one channel. To accomplish this, the balance was placed in a vice to ensure that the balance is level with respect to the loaded channel. A Mitutoyo digital protractor (DP), accurate to .1˚, was used to level the vice. The DP was oriented longitudinally and laterally. Additionally, the DP would be rotated 180˚ in each direction to ensure that the DP read the same value in both directions (see Fig. 2.2)

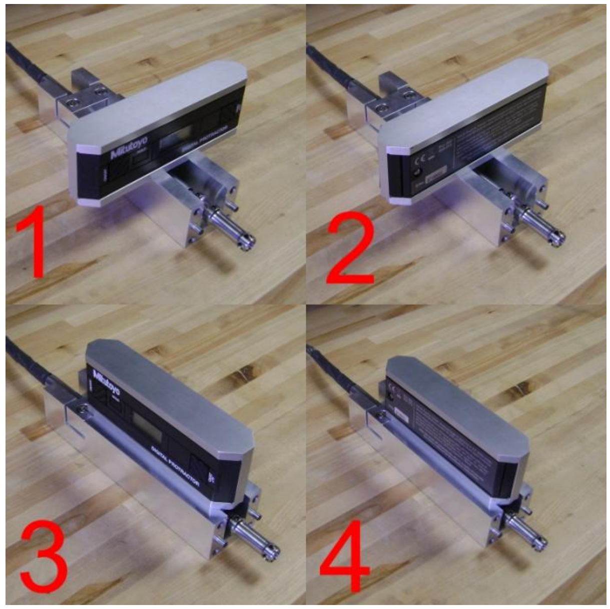

Fig. 2.2

Using the digital level to level the balance. After each step, the vice is adjusted to bring the level to the correct value. Several iterations are performed to until the level reads the same values for steps 1&2 and steps 3&4.

After the balance is sufficiently warmed up and leveled, the data can be gathered using Read_LoadCell_v07.vi[5]. This is a custom made Labview program written by Trenton Carpenter that reads the balance at a settable sample rate and time and saves the average and standard deviation in a text file onto the cRIO.

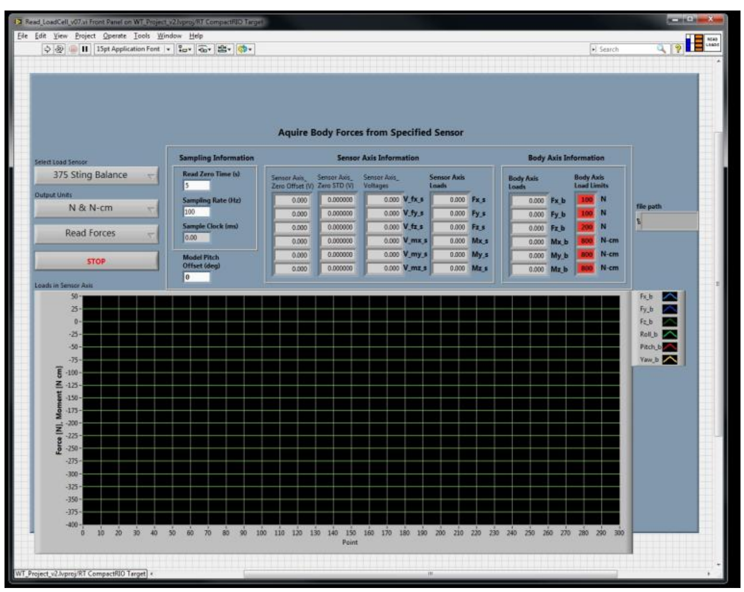

Fig. 2.3

Read_LoadCell_v07.vi[5] Front Panel used for gathering calibration and test data (See Appendix 2 for the block diagram)

The sample rate was set at 100 Hz for 5 seconds, the data saved to the file path C:tmp\sting_balance_data, and accessed via Internet Explorer using ftp://10.0.0.2 as the IP address. Five values for no load were taken in each direction to provide a reference. The VI is then zeroed 5 times and then is loaded in the Fx direction from 0-100g in 10g increments and then up to 250g in 50g increments. The process is repeated 4 more times. After Fx is completed, Fy and Fz are loaded with the same procedure.

Mx has the same load schedule, but requires a custom designed jig (See Fig. 2.4) to apply a pure Mx load without loading any other channels.

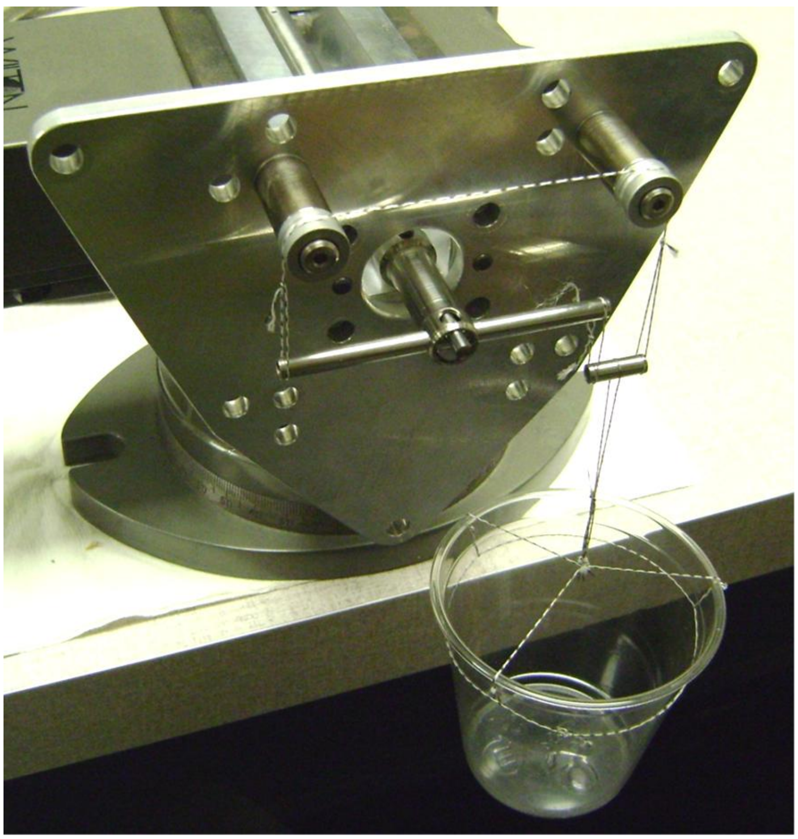

Fig. 2.4

M_x loading jig. Notice that the jig allows for no load imposed on any other channels.

My and Mz were loaded using a different jig (see Fig. 2.5) and loading schedule. First, a datum must be chosen.

Fig. 2.5

M_y/M_z loading jig with datum marked with arrow. Notice that this moment jig imposes a force load in addition to the moment (ie. not a pure moment). While this may not be the ideal case, it is sufficient for our purposes.

The VI is then zeroed and My is loaded with 20 g, 100g, and 200g at 5 different arms; 3.81 cm, 5.08 cm, 6.35 cm, 7.62 cm, and 8.89 cm. Repeat this process 5 times. Mz is loaded with the same procedure.

The slope between the measured voltage and imposed load were calculated in Excel. The slopes of all five trials were averaged and used to populate the 6x6 matrix used in Eq. 1.5. The resulting calibration matrix was then inputted into Voltage2Force_v01.vi[6] which is a sub-VI of a custom made Labview program written by Trenton Carpenter. This sub-VI multiplies the voltage output of the sting balance by the calibration matrix to give a resulting 6x1 matrix of three forces and three moments.

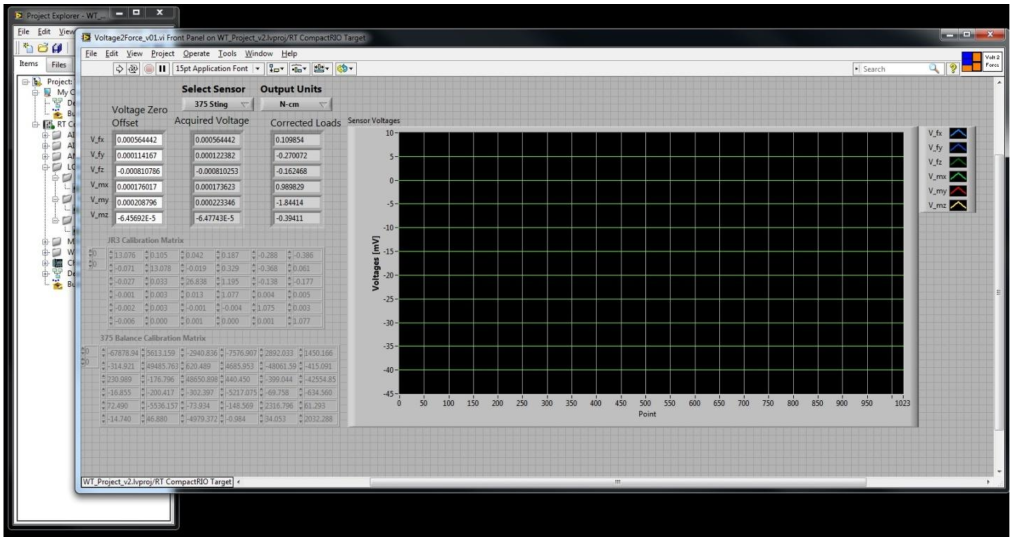

Voltage2Force_v01.vi front panel (see appendix 2 for the block diagram)[6] Fig. 2.6

Analysis of the data to get from voltages to a calibration matrix is discussed in Appendix 3 with the calibration data. After the calibration matrix is finished, the system must be tested, and the error must be estimated. The error analysis is discussed in the discussion section.

The testing procedure is the same procedure as the data acquisition except Read_LoadCell_v03.vi (a sub-VI of WT_Project_v2)[6] is used to collect the data.

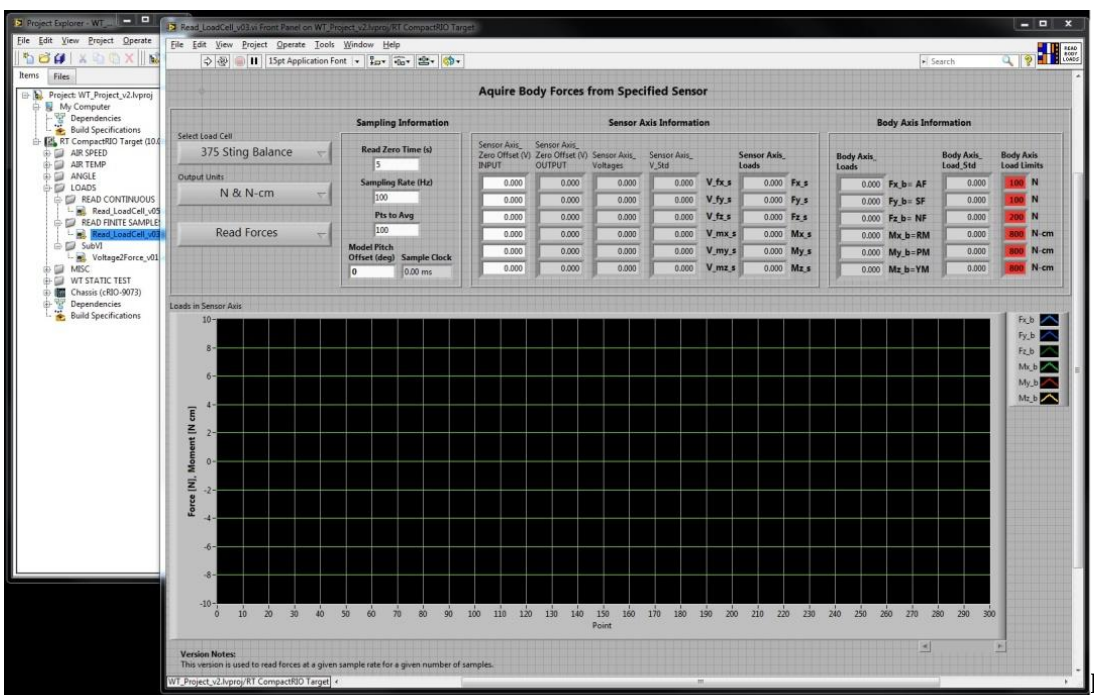

Fig. 2.7

Read_LoadCell_v03.vi front panel (see appendix 2 for the block diagram)[6]

3. Results

3.1. Calibration matrix

See Appendix 3 for data used to find the calibration matrix.

-68725.362	70572.741	-608.535	-5832.989	-24308.328	133.062
-7278.844	583447.882	17524.047	19019.789	-271621.758	-10315.883
358.179	-85569.646	-237901.044	-2826.249	38309.891	120287.584
1.581	-1592.123	-245.894	-5254.389	511.840	-649.803
569.752	-43657.544	-1251.340	-1171.897	18277.205	756.145
4.760	-1182.746	-3797.157	-33.443	535.714	1556.625

Calibration Matrix for Aerolab 375 Sting Balance Fig. 3.1

3.2. Confidence

To within 95% confidence, the average confidence intervals of each channel were calculated, in section 4.3, to be

F_x	+/- .020 N
F_y	+/- .020 N
F_z	+/- .022 N
M_x	+/- .166 Ncm
M_y	+/- .157 Ncm
M_z	+/- .179 Ncm

Average confidence intervals for each channel Fig. 3.2

3.3. Accuracy

The accuracy is calculated and discussed in section 4.4.

F_x	.604 %
F_y	1.662 %
F_z	.904 %
M_x	4.369 %
M_y	12.368 %
M_z	16.414 %

Average percentage error of each channel Fig. 3.3

3.4. Standard Deviation

Averaging the standard deviations of each channel over all 5 trials results in Fig. 3.4.

F_x	+/- .065 N
F_y	+/- .062 N
F_z	+/- .067 N
M_x	+/- .499 Ncm
M_y	+/- .509 Ncm
M_z	+/- .568 Ncm

Chart of channel standard deviations Fig. 3.4

4. Discussion

4.1. Accuracy

The following are the results of the testing procedure to verify the accuracy of the balance and usability of the Labview code. All graphs show the data gathered for the indicated set along with the confidence interval for 95% confidence. The first graph will be the graph with the relevant loads, either the three forces or moments, and the second will be the corresponding moments or forces respectively. Notice the scale at which the second plot is at while analyzing the confidence interval bars.

The first series of data shown corresponds to a pure F_z load.

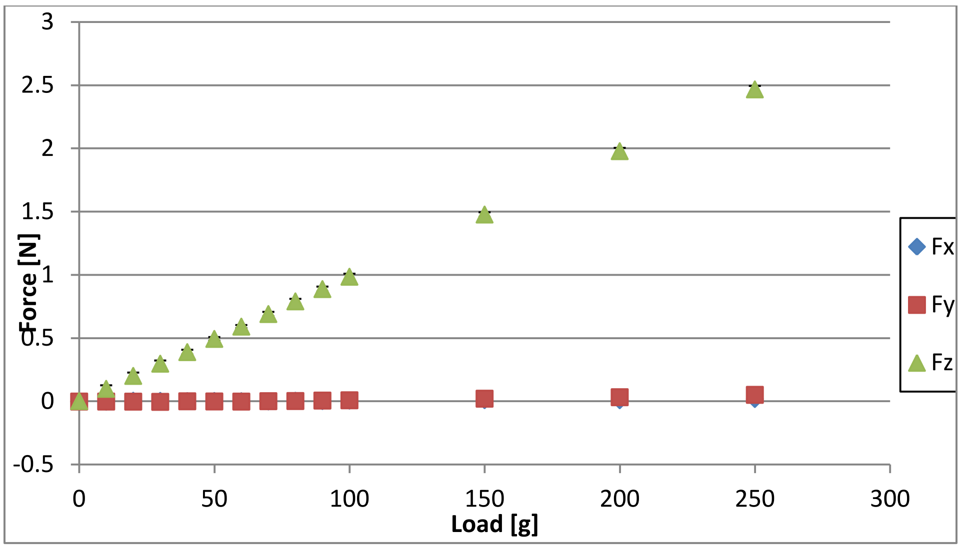

Forces, pure F_z load with confidence interval Fig. 4.1

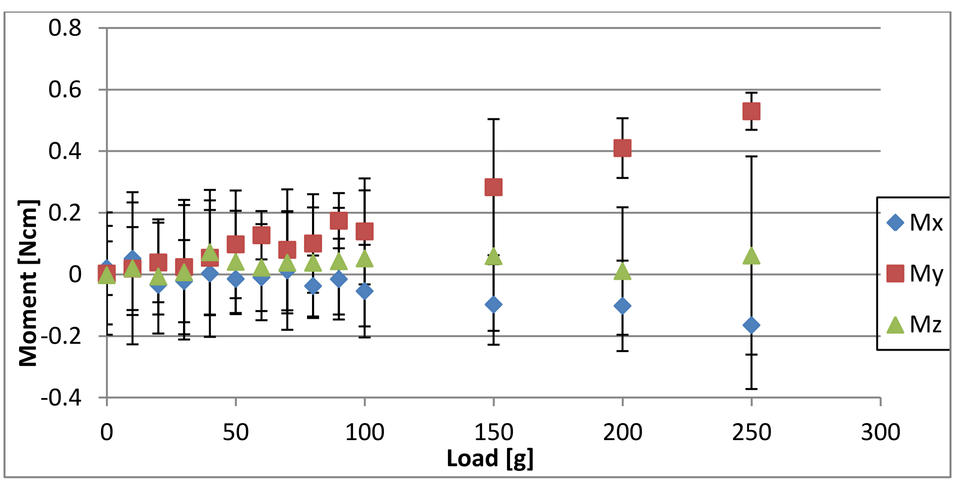

Moments, pure F_z load with confidence interval Fig. 4.2

Above a linear relationship between F_z and the load with a coefficient of correlation (r) of .999 is observed. Additionally, the other force components display 0 within the expected standard deviation for the channel. Looking at the moment data, the x and z components display behavior around 0 that is within the expected standard deviation of the respective channels. The y-component shows virtually no interaction. For the moments, the confidence interval bars are large for two reasons. First, the scale of the graph itself is small because the load is theoretically 0, and secondly, the measured values by the balance are largely random noise leading to a high standard deviation; and therefore a large confidence interval.

Below are the forces and moments due to a pure F_y load.

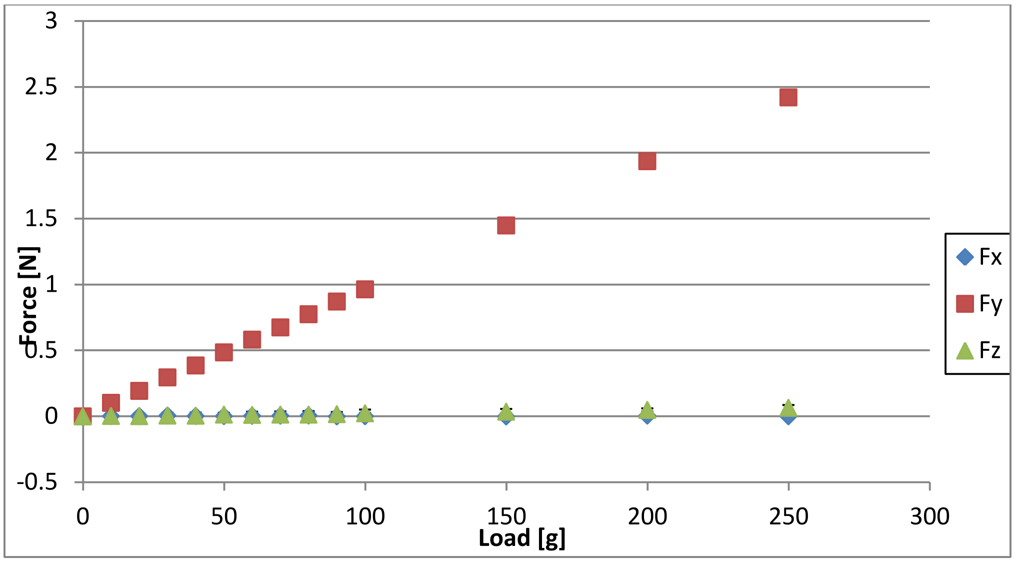

Forces, pure F_y load with confidence interval Fig. 4.3

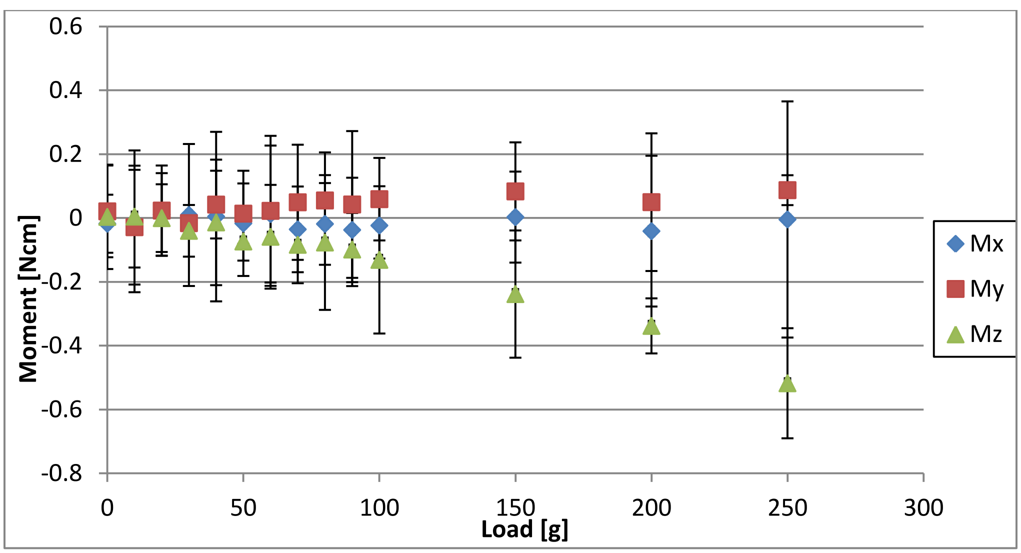

Moments, pure F_y load with confidence interval Fig. 4.4

Similar behavior can be seen with the data resulting from the pure F_y load where r=.999. There is an unclear dependence between F_y and M_z. M_z does trend toward a negative dependence, but again, the values negligible and within the standard deviation of the channel.

Below are the forces and moments due to a pure F_x load.

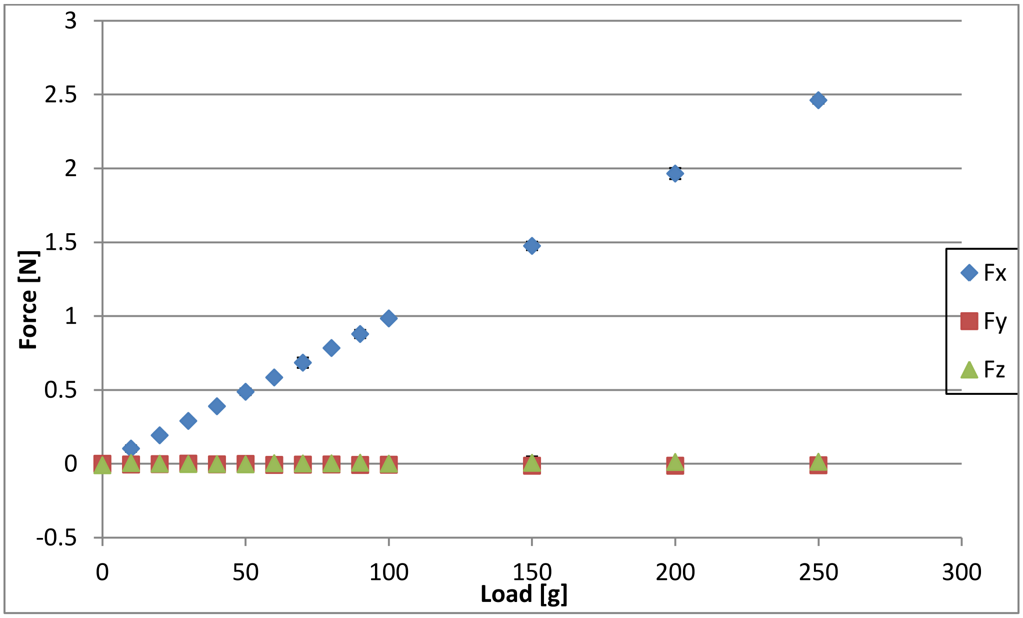

Forces, pure F_x load with confidence interval Fig. 4.5

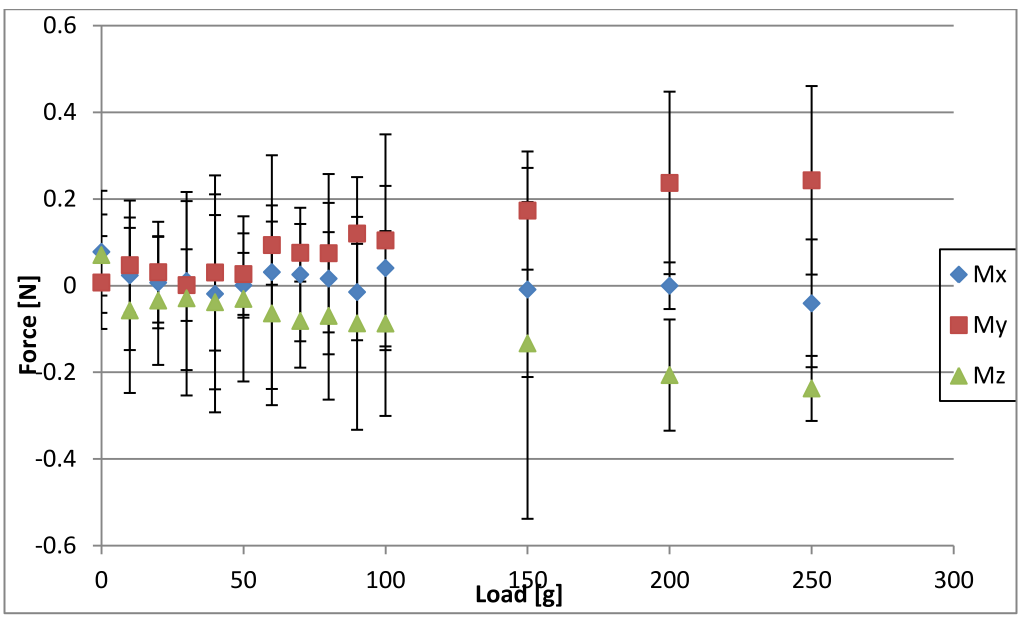

Moments, pure F_x load with confidence interval Fig. 4.6

A pure x component force load again shows very similar behavior as the previous two loading conditions with r=.999, but this time no dependence between F_x and any moment channel is observed.

Below are the forces and moments due to a pure M_x load.

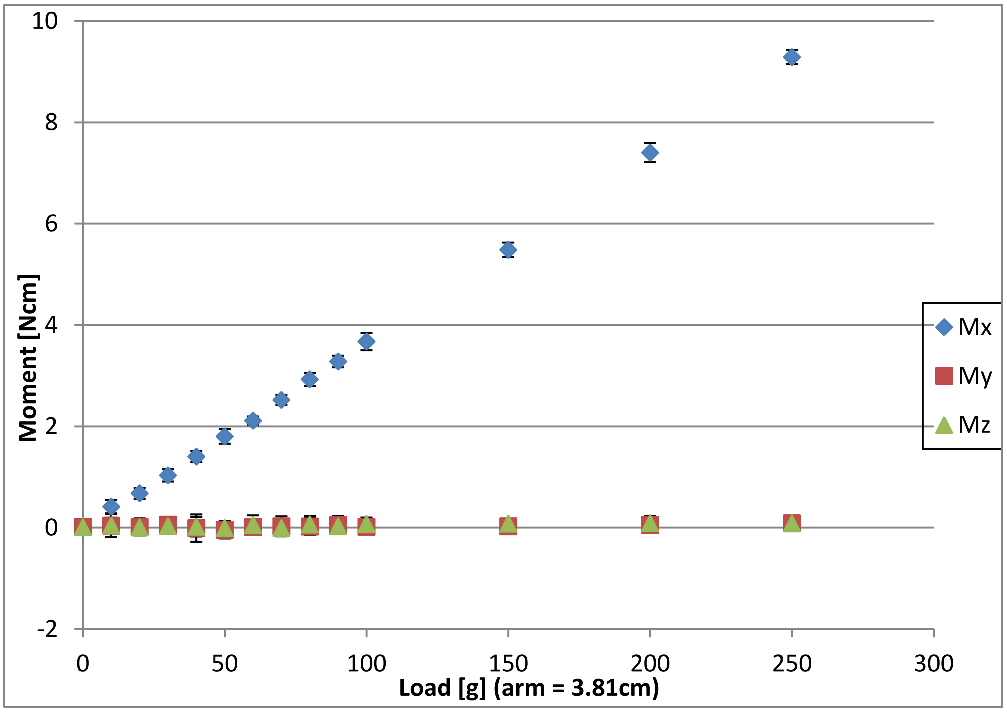

Moments, pure M_x load with confidence interval Fig. 4.7

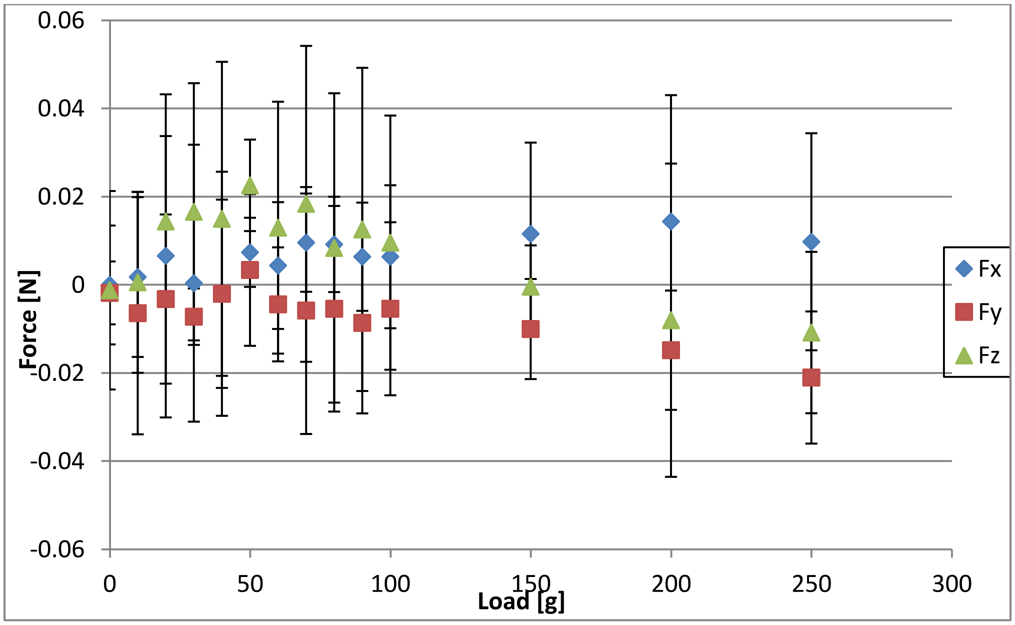

Forces, pure M_x load with confidence interval Fig. 4.8

A pure M_x load yields a well defined linear relationship, r=.999, with M_x and acceptable values of 0 for both the other moment channels and all of the force channels.

Below are the forces and moments due to a combined M_z and F_z load.

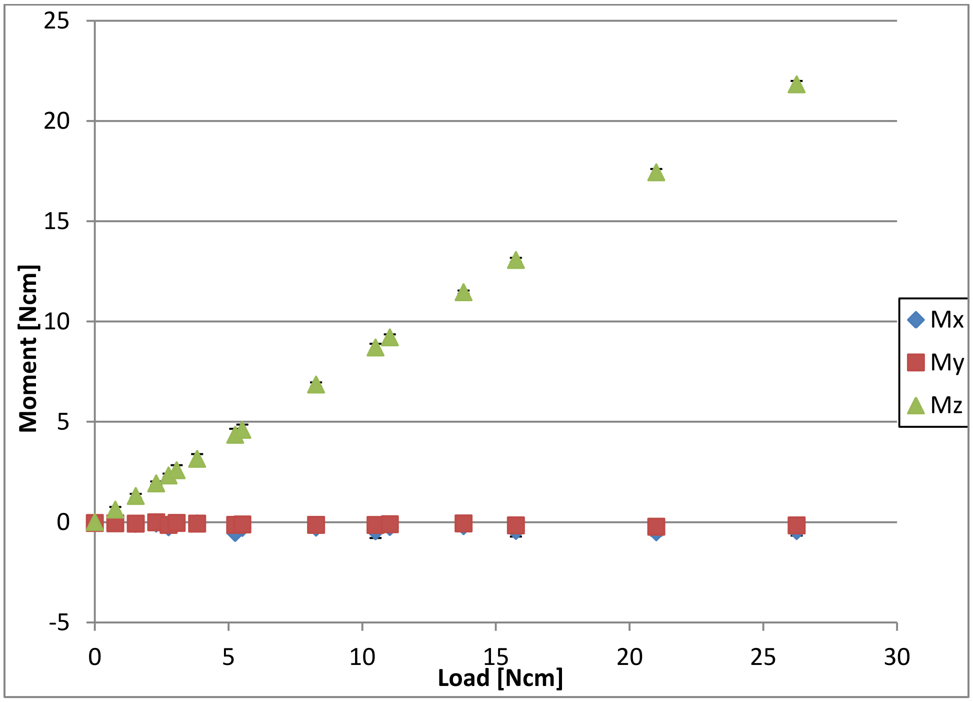

Moments, M_z and F_z load with confidence interval Fig. 4.9

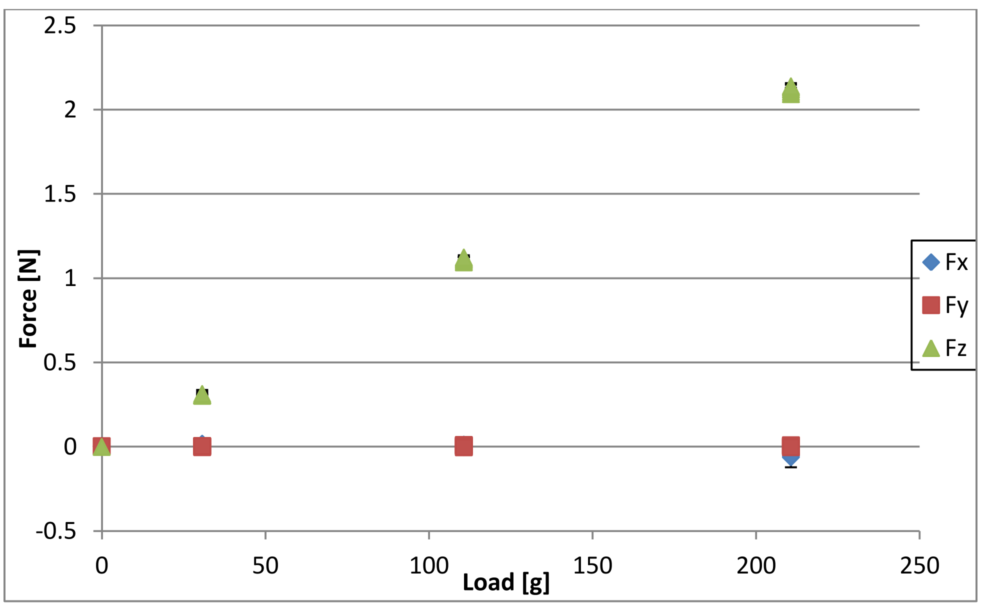

Forces, M_z and F_z load with confidence interval Fig. 4.10

Above we can see a linear relationship between the applied load and M_z, r=.999, with the other loads being within the 0 range. Recall that pure M_z and M_y loads could not be produced, and to produce the moment loads, a force load was imposed on the balance. A linear relationship between F_z and the applied force is observed where the coefficient of correlation is .999. Additionally, the other channels report acceptable values of 0 thereby verifying the balance's capability of measuring simultaneous forces and moments of the same component.

Below are the forces and moments due to a combined M_y and F_y load.

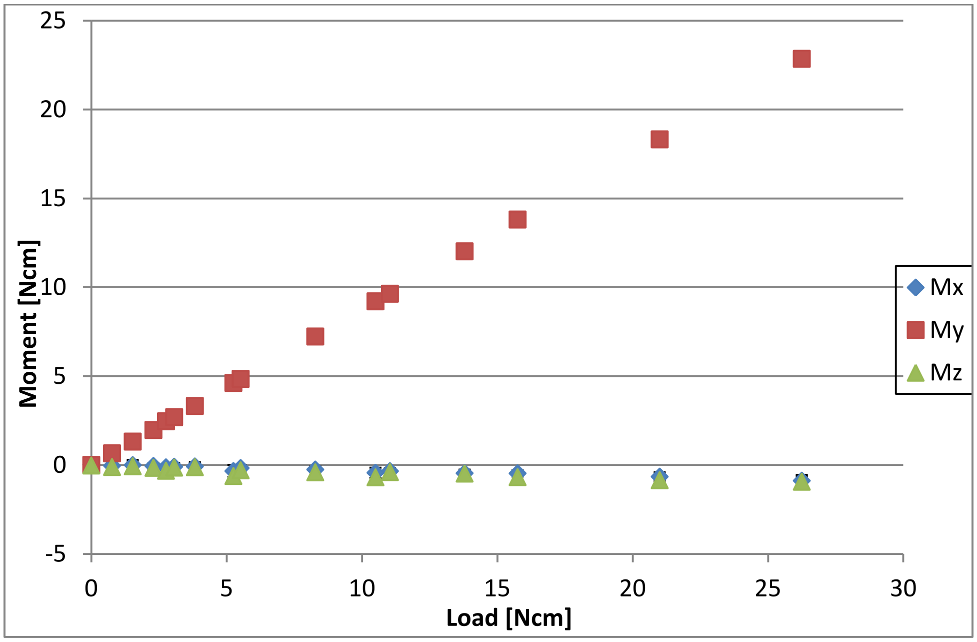

Moments, M_y and F_y load with confidence interval Fig. 4.11

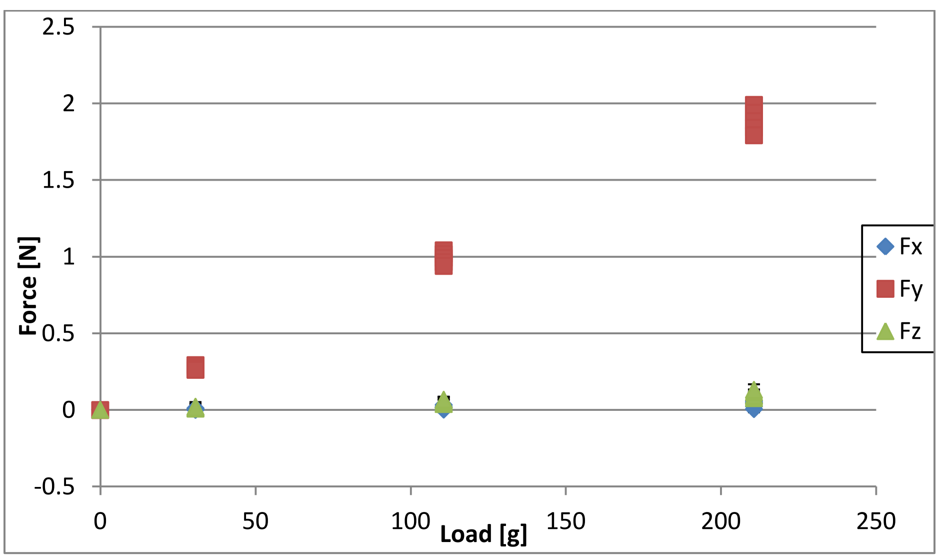

Forces, M_y and F_y load with confidence interval Fig. 4.12

The y component values of moment and force display similar behavior to the z components. r=.999 & .998 for the moments and forces respectively. For both the M_z and M_y cases, a slight negative dependence could be made out with the other two moment channels, but they are not far enough from 0 to call them anything else but noise.

The accuracy was found by taking the average value of a loaded channel and comparing to it the nominal value though the following equation.

$$Accuracy = \frac{(Measure\ \ value\ - True\ value)}{True\ value} \cdot 100 \qquad \text{Eq. 4.2}$$

Load [g]	Force [N]	Fz	% error	Fy	% error	Fx	% error
0	0.000	0.001		-0.0022		0.0008	
10	0.098	0.098	0.510	0.1008	2.752	0.1042	6.218
20	0.196	0.200	1.733	0.1914	2.446	0.1938	1.223
30	0.294	0.296	0.714	0.2938	0.170	0.2912	1.053
40	0.392	0.388	1.172	0.3844	2.039	0.3906	0.459
50	0.491	0.492	0.387	0.4836	1.407	0.4886	0.387
60	0.589	0.589	0.136	0.5802	1.427	0.5856	0.510
70	0.687	0.689	0.306	0.6732	1.966	0.6856	0.160
80	0.785	0.789	0.561	0.773	1.504	0.7848	0.000
90	0.883	0.886	0.396	0.8694	1.529	0.8798	0.351
100	0.981	0.984	0.326	0.962	1.937	0.9852	0.428
150	1.472	1.476	0.292	1.447	1.665	1.4764	0.333
200	1.962	1.977	0.775	1.9346	1.397	1.9662	0.214
250	2.453	2.466	0.542	2.419	1.366	2.4626	0.412
Average Error			0.604		1.662		0.904

Percentage of error for the force channels Fig. A4.1

Load [g]	Force [N]	Moment [Ncm]	Mx	% error
0	0.000	0.000	-0.0056	
10	0.098	0.374	0.4164	11.408
20	0.196	0.748	0.6814	8.845
30	0.294	1.121	1.0332	7.856
40	0.392	1.495	1.4042	6.076
50	0.491	1.869	1.8026	3.543
60	0.589	2.243	2.1154	5.671
70	0.687	2.616	2.5226	3.582
80	0.785	2.990	2.9294	2.030
90	0.883	3.364	3.2816	2.445
100	0.981	3.738	3.676	1.648
150	1.472	5.606	5.4864	2.141
200	1.962	7.475	7.4044	0.947
250	2.453	9.344	9.2874	0.606
Average Error				4.369

Percentage error for the M_x channel (arm = 3.81cm) Fig. A4.2

Mass (g)	Arm (cm)	Moment (Ncm)	My	% error	Mz	% error
0	0	0.000	0.0088		0.013	
30.715	2.54	0.765	0.6602	13.737	0.634	17.135
30.715	5.08	1.531	1.3208	13.711	1.312	14.312
30.715	7.62	2.296	1.9742	14.016	1.940	15.506
110.715	2.54	2.759	2.4618	10.763	2.334	15.396
30.715	10.16	3.061	2.6946	11.980	2.596	15.207
30.715	12.7	3.827	3.3266	13.068	3.164	17.312
210.715	2.54	5.250	4.6216	11.977	4.363	16.906
110.715	5.08	5.517	4.85	12.097	4.610	16.454
110.715	7.62	8.276	7.2346	12.585	6.868	17.020
210.715	5.08	10.501	9.213	12.265	8.716	16.996
110.715	10.16	11.035	9.6426	12.617	9.222	16.429
110.715	12.7	13.794	12.0272	12.806	11.471	16.839
210.715	7.62	15.751	13.8176	12.277	13.078	16.973
210.715	10.16	21.002	18.3258	12.742	17.450	16.911
210.715	12.7	26.252	22.8584	12.928	21.837	16.820
Average Error				12.638		16.414

Percentage error for M_y and M_z channels Fig. A4.3

4.2. Standard Deviation

Recall that the Labview program takes 500 samples each time a measurement is taken and then displays and average and standard deviation of these values. The resolution of the balance was determined by calculating the average the standard deviations for each channel over the 30 test trials.

	Fx STD	FY STD	FZ STD	Mx STD	My STD	Mz STD
Average STD	0.065	0.062	0.067	0.499	0.509	0.568
Std	0.003	0.003	0.002	0.017	0.014	0.023

Standard deviation data Fig. 4.16

4.3. Confidence Interval

$$Confidence\ \ Interval = M \pm t \cdot \sigma \qquad \text{Eq. 4.1}$$

Where for 95% confidence and a population of 5 gives t = 2.571[10].

Each data value has a confidence interval that was calculated for it. For simplicity sake, the average confidence interval for each loading condition was found and is displayed below.

Channel	Fx (AF)	Fy (SF)	Fz (NF)	Mx (RM)	My (PM)	Mz (YM)
Average Confidence Interval	0.016	0.022	0.021	0.144	0.151	0.202

Average confidence intervals for F_z load Fig. 4.17

Channel	Fx (AF)	Fy (SF)	Fz (NF)	Mx (RM)	My (PM)	Mz (YM)
Average Confidence Interval	0.018	0.016	0.019	0.185	0.145	0.147

Average confidence intervals for F_y loads Fig. 4.18

Channel	Fx (AF)	Fy (SF)	Fz (NF)	Mx (RM)	My (PM)	Mz (YM)
Average Confidence Interval	0.022	0.018	0.020	0.162	0.141	0.188

Average confidence intervals for F_x loads Fig. 4.19

Channel	Fx (AF)	Fy (SF)	Fz (NF)	Mx (RM)	My (PM)	Mz (YM)
Average Confidence Interval	0.019	0.018	0.026	0.130	0.147	0.131

Average confidence intervals M_x loads Fig. 4.20

Channel	Fx (AF)	Fy (SF)	Fz (NF)	Mx (RM)	My (PM)	Mz (YM)
Average Confidence Interval	0.025	0.021	0.016	0.173	0.171	0.154

Average confidence intervals M_y loads Fig. 4.21

Channel	Fx (AF)	Fy (SF)	Fz (NF)	Mx (RM)	My (PM)	Mz (YM)
Average Confidence Interval	0.021	0.023	0.026	0.203	0.185	0.253

Average confidence intervals M_z loads Fig. 4.22

5. Conclusion

The calibration matrix for the Aerolab 375 sting balance is experimentally estimated to be

-68725.362	70572.741	-608.535	-5832.989	-24308.328	133.062
-7278.844	583447.882	17524.047	19019.789	-271621.758	-10315.883
358.179	-85569.646	-237901.044	-2826.249	38309.891	120287.584
1.581	-1592.123	-245.894	-5254.389	511.840	-649.803
569.752	-43657.544	-1251.340	-1171.897	18277.205	756.145
4.760	-1182.746	-3797.157	-33.443	535.714	1556.625

Calibration Matrix for Aerolab 375 Sting Balance. The first three columns have units of N and the second three columns have units of Ncm. Fig. 5.1

To within 95% confidence, the average confidence intervals of each channel were calculated to be

F_x	+/- .020 N
F_y	+/- .020 N
F_z	+/- .022 N
M_x	+/- .166 Ncm
M_y	+/- .157 Ncm
M_z	+/- .179 Ncm

Average confidence intervals for each channel Fig. 5.2

to within an approximate error of

F_x	.604 %
F_y	1.662 %
F_z	.904 %
M_x	4.369 %
M_y	12.368 %
M_z	16.414 %

Average percentage error of each channel Fig. 5.3

And a standard deviation of

F_x	+/- .065 N
F_y	+/- .062 N
F_z	+/- .067 N
M_x	+/- .499 Ncm
M_y	+/- .509 Ncm
M_z	+/- .568 Ncm

Chart of channel standard deviations Fig. 5.4

The goal of the project was to find a calibration matrix that 1.) converts the voltage output of the sting balance to meaningful force and moment data, 2.) eliminates or reduces to a negligible effect the interactions between channels, and finally 3.) to determine the accuracy of the balance. Fig. 5.1 shows a calibration matrix that provides meaningful values from our sting balance and reduces the dependencies to a negligible effect. However, this method does display a standard deviation of around .065 N and .5 Ncm which limits the size of the models that can be testing with this balance. Operating the balance on the low end of the range of forces and moments accounts for some of the decreased accuracy. Also, a slight interaction, within the standard deviation of the balance, can be noticed with some of the moment channels. Not being able to apply a pure M_y and M_z load is a significant problem in this method and is likely the result of a small interaction in some of the moment channels.

5.1. Further Work

To further improve upon what has been done here, expanding the calibration range by 1 to 1.5N would decrease or eliminate the small dependencies that begin to develop on the upper ends of the current calibration range. This would be the simplest way to increase the accuracy and usability of the balance. Also, a jig to apply a pure load to each channel should be built. After this is accomplished, the method outlined in this thesis should be repeated and the new data used to calibrate the balance. Another way to further improve the accuracy of the system would be to account for second order interactions. This would involve loading two channels simultaneously and using that data to find a 12x12 calibration matrix. Noting the accuracy found in this method though, the benefits of gained from a matrix accounting for second order interactions is likely negligible for the purposes of this balance.

Appendix 1 – Sting Balance Equation

The sting balance gives out 6 voltages labeled N1, N2, S1, S2, R, and A. A more useful output is data in the form of forces or moments namely D, L, S, R, P, Y (not respective to the above voltages). Relating the voltage to a force or moment is done by taking data and finding a relationship between the measured value, the voltage, and the known value, the imposed load, over several different values to give a slope in terms of Voltage/Force or Moment. In a one dimensional case the reverse relationship can simply be found by inverting this slope. In principal, the 6 dimensional case presented here is the same, but with a small variation to preserve the correct units.

The input vector into the calibration equation (the 1x6 voltage vector given from the balance) is

$$\begin{bmatrix} A & \mathrm{N1} & \mathrm{S1} & R & N2 & S2 \end{bmatrix} \qquad \text{Eq. A1.1}$$

And the desired output vector is

$$\begin{bmatrix} \mathrm{D} & L & S & \mathrm{R} & \mathrm{P} & \mathrm{Y} \end{bmatrix}^T \qquad \text{Eq. A1.2}$$

The slopes given by the calibration data can be represented in a 6x6 matrix by

$$\begin{bmatrix} m_{\mathrm{D},A} & m_{\mathrm{D},N1} & m_{\mathrm{D},S1} & m_{\mathrm{D},R} & m_{\mathrm{D},N2} & m_{\mathrm{D},S2} \\ m_{L,A} & m_{L,N1} & m_{L,S1} & m_{L,R} & m_{L,N2} & m_{L,S2} \\ m_{S,A} & m_{S,N1} & m_{S,S1} & m_{S,R} & m_{S,N2} & m_{S,S2} \\ m_{R,A} & m_{R,N1} & m_{R,S1} & m_{R,R} & m_{R,N2} & m_{R,S2} \\ m_{P,A} & m_{P,N1} & m_{P,S1} & m_{P,R} & m_{P,N2} & m_{P,S2} \\ m_{Y,A} & m_{Y,N1} & m_{Y,S1} & m_{Y,R} & m_{Y,N2} & m_{Y,S2} \end{bmatrix} \qquad \text{Eq. A1.3}$$

Where m is a slope with the first index as the loading condition, and the second index as the resulting voltage. The first three rows of this matrix have units of V/N, and the last three rows' units are V/Ncm. First, the relationship must be reversed so that the voltage vector multiplied by the calibration matrix will give a force or moment:

$$\left(\begin{bmatrix} m_{\mathrm{D},A} & m_{\mathrm{D},N1} & m_{\mathrm{D},S1} & m_{\mathrm{D},R} & m_{\mathrm{D},N2} & m_{\mathrm{D},S2} \\ m_{L,A} & m_{L,N1} & m_{L,S1} & m_{L,R} & m_{L,N2} & m_{L,S2} \\ m_{S,A} & m_{S,N1} & m_{S,S1} & m_{S,R} & m_{S,N2} & m_{S,S2} \\ m_{R,A} & m_{R,N1} & m_{R,S1} & m_{R,R} & m_{R,N2} & m_{R,S2} \\ m_{P,A} & m_{P,N1} & m_{P,S1} & m_{P,R} & m_{P,N2} & m_{P,S2} \\ m_{Y,A} & m_{Y,N1} & m_{Y,S1} & m_{Y,R} & m_{Y,N2} & m_{Y,S2} \end{bmatrix}\right)^{-1} \qquad \text{Eq. A1.4}$$

But notice that the first three and second three rows are now N/V and Ncm/V respectively. If we were to perform matrix multiplication with Eq. A1.1 and Eq. A1.4, the units of each value in the resulting 6x1 matrix would be attempting to add N and Ncm; an operation which does not make physical sense. To alleviate this issue, the transpose of Eq. A1.4 is taken:

$$\left(\begin{bmatrix} m_{D,A} & m_{D,N1} & m_{D,S1} & m_{D,R} & m_{D,N2} & m_{D,S2} \\ m_{L,A} & m_{L,N1} & m_{L,S1} & m_{L,R} & m_{L,N2} & m_{L,S2} \\ m_{S,A} & m_{S,N1} & m_{S,S1} & m_{S,R} & m_{S,N2} & m_{S,S2} \\ m_{R,A} & m_{R,N1} & m_{R,S1} & m_{R,R} & m_{R,N2} & m_{R,S2} \\ m_{P,A} & m_{P,N1} & m_{P,S1} & m_{P,R} & m_{P,N2} & m_{P,S2} \\ m_{Y,A} & m_{Y,N1} & m_{Y,S1} & m_{Y,R} & m_{Y,N2} & m_{Y,S2} \end{bmatrix}^{-1}\right)^{T} \qquad \text{Eq. A1.5}$$

Which now gives the first three columns units of N/V, and the second three columns units of Ncm/V, so that

$$\begin{bmatrix} A & N1 & S1 & R & N2 & S2 \end{bmatrix}\left(\begin{bmatrix} m_{D,A} & m_{D,N1} & m_{D,S1} & m_{D,R} & m_{D,N2} & m_{D,S2} \\ m_{L,A} & m_{L,N1} & m_{L,S1} & m_{L,R} & m_{L,N2} & m_{L,S2} \\ m_{S,A} & m_{S,N1} & m_{S,S1} & m_{S,R} & m_{S,N2} & m_{S,S2} \\ m_{R,A} & m_{R,N1} & m_{R,S1} & m_{R,R} & m_{R,N2} & m_{R,S2} \\ m_{P,A} & m_{P,N1} & m_{P,S1} & m_{P,R} & m_{P,N2} & m_{P,S2} \\ m_{Y,A} & m_{Y,N1} & m_{Y,S1} & m_{Y,R} & m_{Y,N2} & m_{Y,S2} \end{bmatrix}^{-1}\right)^{T} = \begin{bmatrix} D \\ L \\ S \\ R \\ P \\ Y \end{bmatrix} \qquad \text{Eq. A1.6}$$

Where D, L, and S are drag, lift, and side forces with units of N; and R, P, and Y are roll, pitch, and yaw moments with units of Ncm.

Appendix 2 – Labview code

The following are the custom made Labview programs written for the Advanced Mechanics and Composite Technology Lab written by Trenton Carpenter. All file paths are for the computer labeled BAT-042-4.

Read_LoadCell_v07.vi[5]
File path: C:_OSU windtunnel\Projects\Sting Balance\Sting Balance

This program is used to gather the initial calibration data. A sample rate and time are set to read a finite amount of samples, and then the average and standard deviation are saved in a text format on the cRIO to the file path ftp:\\10.0.0.2.

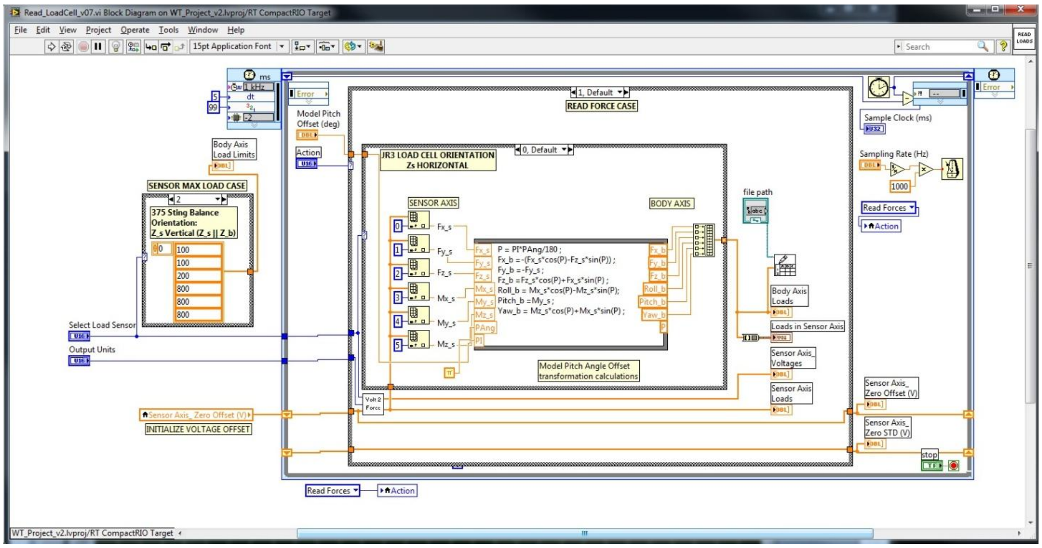

Read_LoadCell_v07.vi block diagram to read forces[5] Fig. A2.1

The following is a sub-program which determines the average that the balance is reading over a given sample rate and time and subtracts that value from what is read; thereby zeroing the balance.

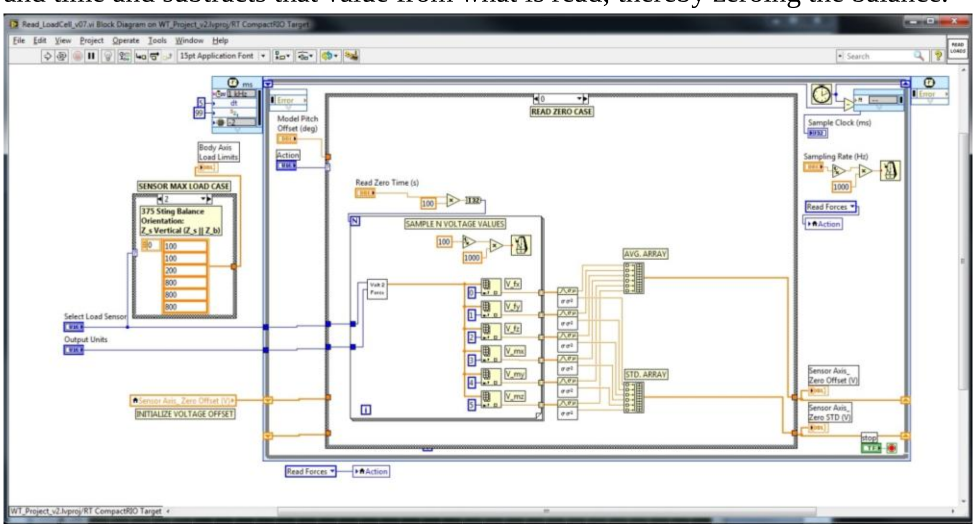

Read_LoadCell_v07.vi block diagram to read zero[6] Fig. A2.2

WT_Project_v2.vi[6]

File path: C:_OSU Windtunnel\Labview\VI_Development\Wind Tunnel Project_labview 2010

WT_project_v2.vi is the main Labview program used in the wind tunnel. This specific sub-program takes the voltages read from the balance at a given sample rate and time, finds the average and standard deviation, multiplies these by the calibration matrix, and then saves the data to on the cRIO.

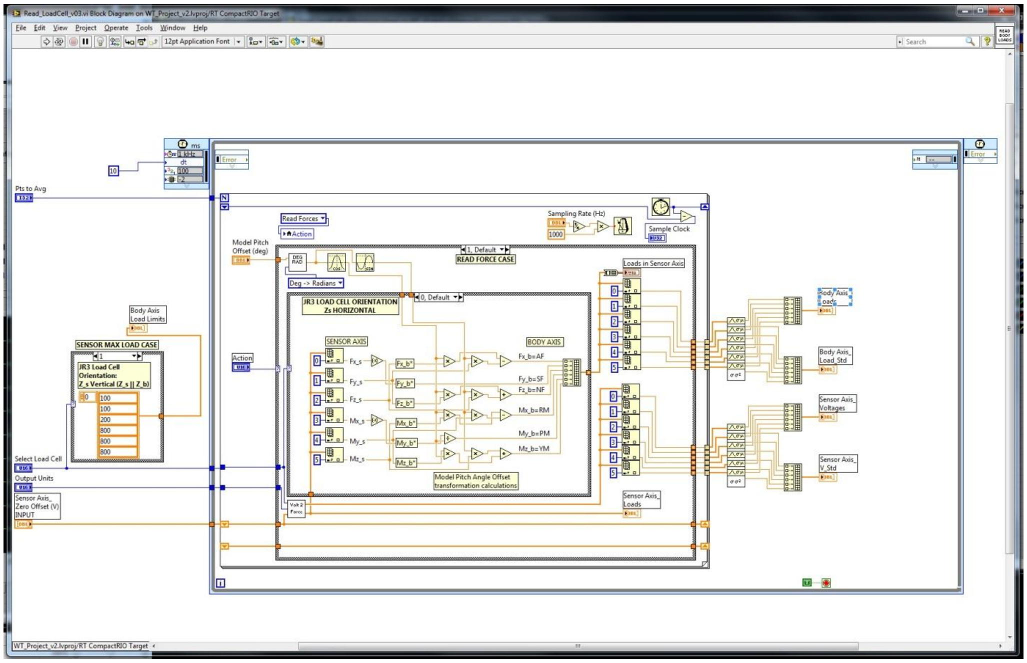

Read_LoadCell_v03.vi block diagram read forces[6] Fig. A2.6

The program below zeros the balance for Read_LoadCell_v03.vi.

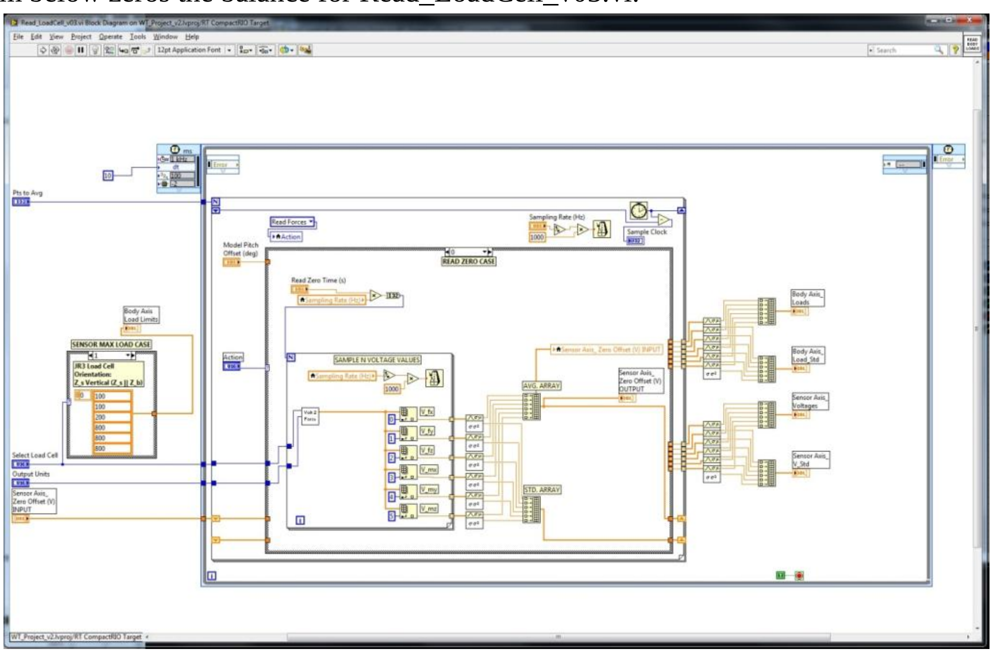

Read_LoadCell_v03.vi block diagram read 0[6] Fig. A2.7

The calibration matrix is entered into this SubVI to convert the voltages to forces and moments.

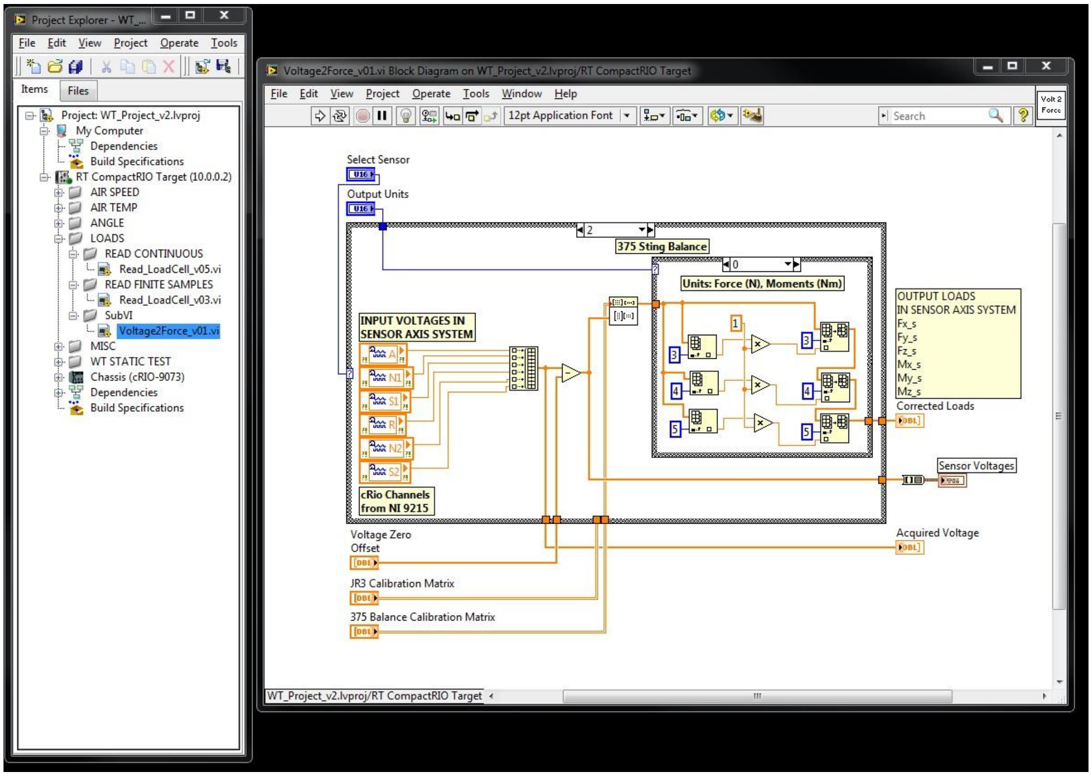

Voltage2Force_v01.vi block diagram.vi block diagram[6] Fig. A2.9

The final VI here reads the balance continuously. While this program was not discussed in the work above, it was extensively used to test the balance and calibration matrix to see if the resulting values were reasonable before taking large data sets. It also has many applications in the wind tunnel as it live feeds the data coming off the balance at the given sample rate.

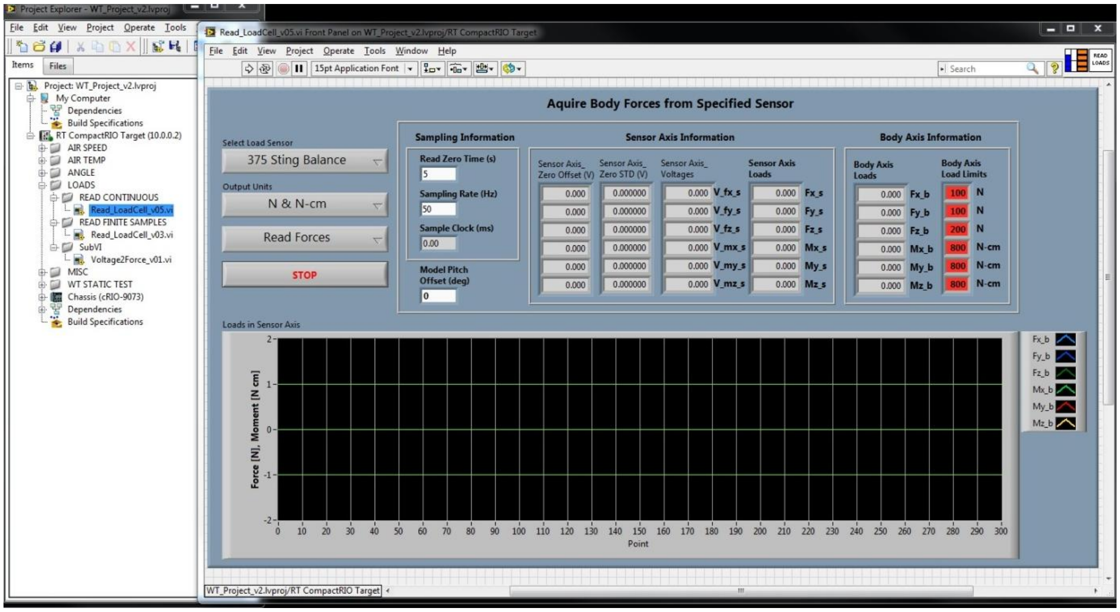

Read_LoadCell_v05 front panel read continuous[6] Fig. A2.3

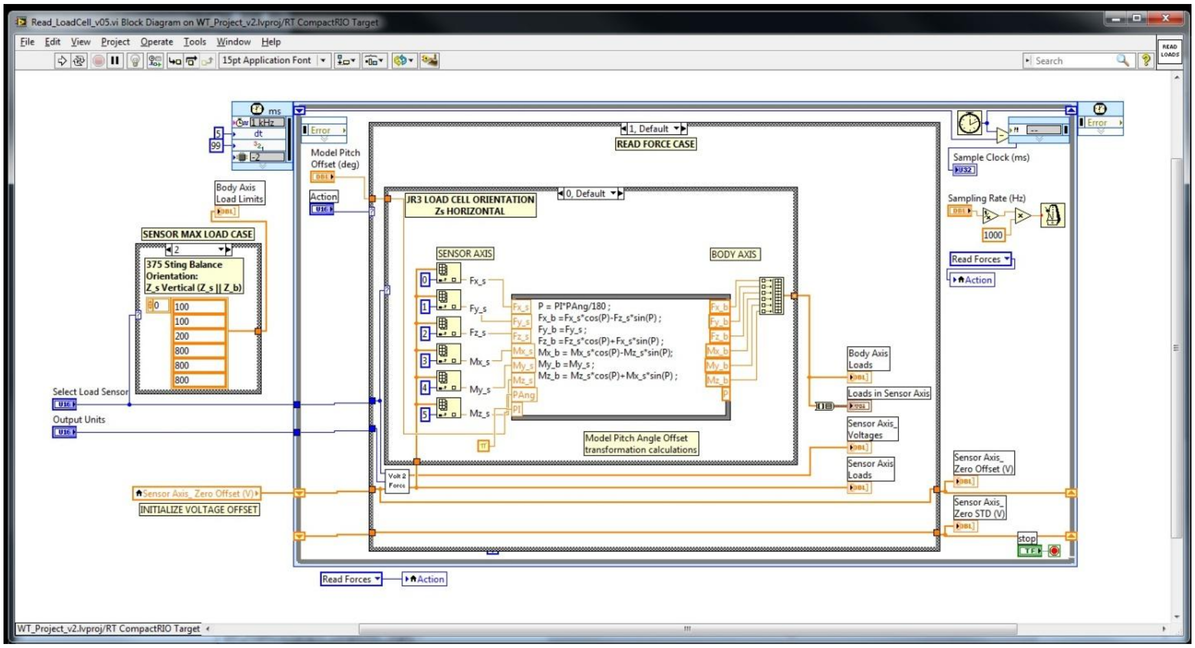

Read_LoadCell_v05 block diagram read continuous[6] Fig. A2.4

Below is the zero setting case for the continuous read VI.

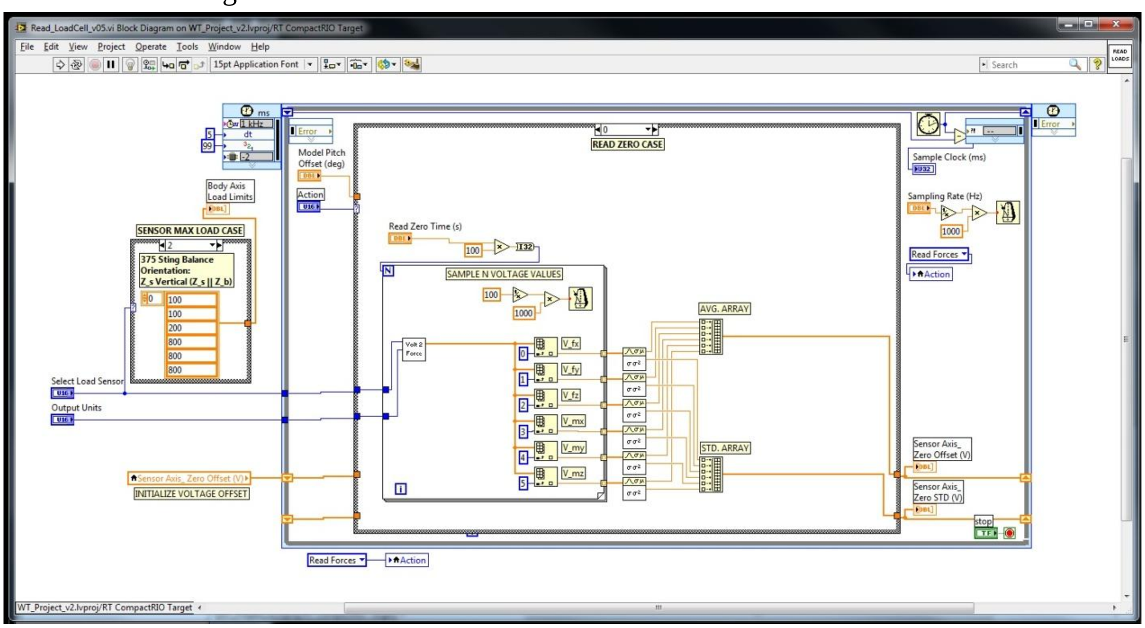

Read_LoadCell_v05.vi block diagram read 0[6] Fig. A2.4

Appendix 3 – Calibration data

This appendix shows the data used to find the calibration matrix. Each table consists of the value for each channel and load averaged over the 5 trials and the slopes used to populate the calibration matrix equation (Eq. 1.5).

F_y data

Mass	N1	N2	S1	S2	R	A
0.00E+00	-1.74E-07	1.99E-07	-8.83E-08	2.19E-07	9.82E-07	1.63E-07
1.00E+01	-2.36E-06	-3.45E-06	-1.81E-07	7.07E-07	-7.45E-08	-3.43E-07
2.00E+01	-2.72E-06	-7.00E-06	-4.54E-07	2.62E-07	9.40E-07	-9.72E-07
3.00E+01	-4.78E-06	-9.94E-06	2.74E-08	-8.88E-07	2.89E-07	-1.28E-06
4.00E+01	-6.29E-06	-1.28E-05	1.15E-07	3.47E-07	2.07E-07	-1.61E-06
5.00E+01	-8.42E-06	-1.71E-05	-4.61E-07	3.28E-08	1.12E-06	-1.73E-06
6.00E+01	-8.89E-06	-2.04E-05	-3.11E-07	7.65E-07	4.09E-07	-2.62E-06
7.00E+01	-1.11E-05	-2.40E-05	-6.06E-07	1.80E-07	8.68E-07	-3.00E-06
8.00E+01	-1.17E-05	-2.74E-05	-3.82E-07	1.37E-08	3.27E-07	-2.65E-06
9.00E+01	-1.44E-05	-3.13E-05	-4.43E-07	9.08E-07	1.08E-06	-2.87E-06
1.00E+02	-1.48E-05	-3.47E-05	3.20E-07	-3.42E-07	1.17E-06	-3.52E-06
1.50E+02	-2.31E-05	-5.34E-05	-1.01E-06	-2.34E-07	2.01E-06	-4.39E-06
1.98E+02	-2.97E-05	-6.97E-05	-8.48E-07	3.11E-07	2.92E-06	-5.78E-06
2.38E+02	-3.62E-05	-8.48E-05	-1.06E-06	2.57E-08	2.59E-06	-7.23E-06
Slope [V/g]	-1.50295E-07	-3.6E-07	-4.1E-09	-7.2E-10	1.1E-08	-2.9E-08

Table of voltages measured from various pure F_y loads Fig. A4.1

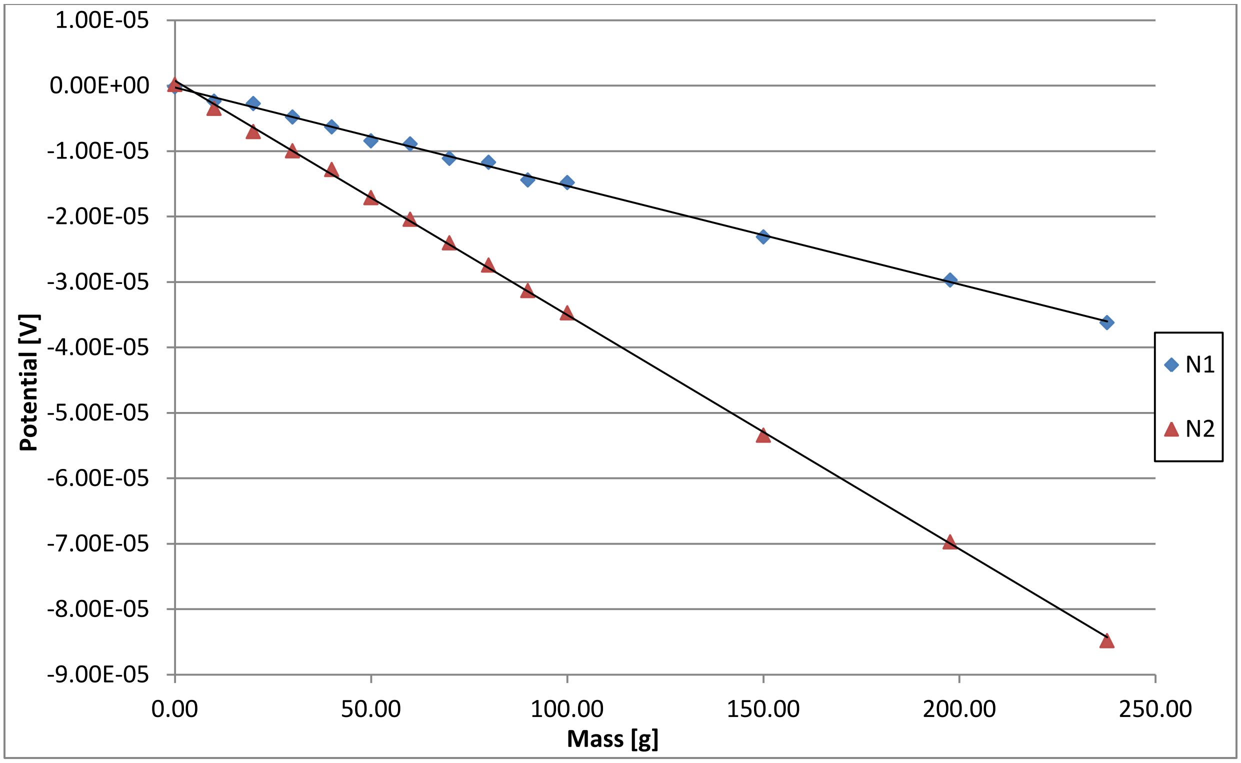

N_1 and N_2 voltages with pure F_y load Fig. A4.2

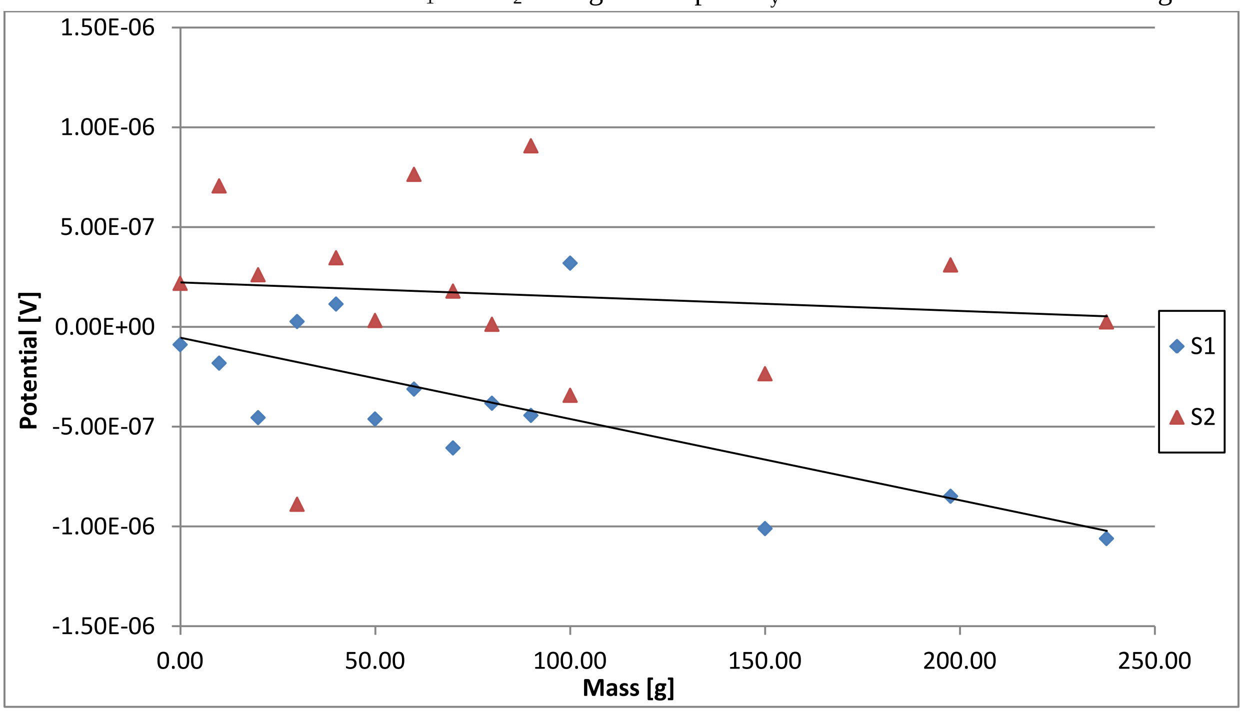

S_1 and S_2 voltages with pure F_y load Fig. A4.3

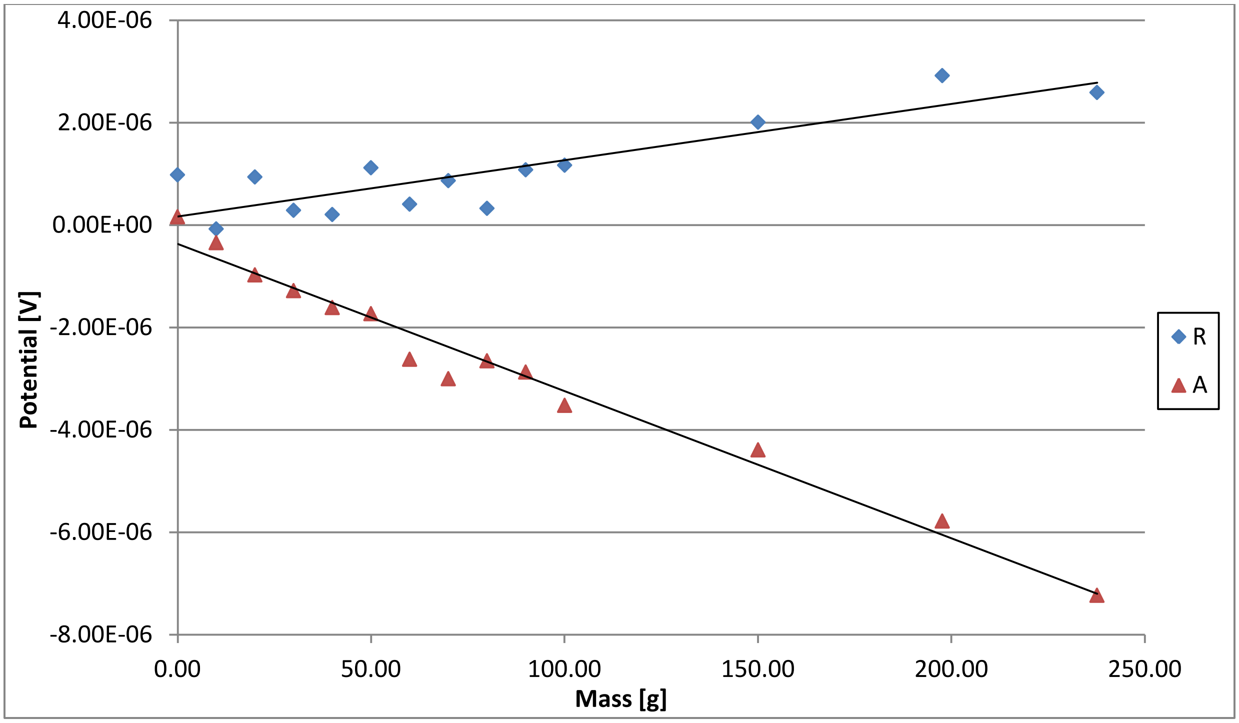

R and A voltages with pure F_y load Fig. A4.4

F_z data

Mass	N1	N2	S1	S2	R	A
0.00E+00	-1.32E-06	7.75E-08	-4.50E-07	3.52E-08	1.12E-06	-4.58E-07
1.00E+01	-2.81E-07	-3.30E-07	1.40E-06	4.91E-06	-9.88E-07	-7.93E-07
2.00E+01	-1.56E-06	3.78E-07	3.38E-06	8.75E-06	-1.72E-06	-7.15E-07
3.00E+01	-1.15E-06	-7.24E-07	4.72E-06	1.25E-05	-1.44E-06	-4.59E-07
4.00E+01	-1.24E-06	-8.47E-07	6.39E-06	1.67E-05	-2.14E-06	-1.71E-07
5.00E+01	-9.70E-07	-9.26E-07	8.06E-06	2.19E-05	-2.74E-06	-6.16E-07
6.00E+01	-9.25E-07	-3.81E-07	1.03E-05	2.56E-05	-3.64E-06	-1.72E-07
7.00E+01	-1.48E-06	-1.01E-06	1.16E-05	3.07E-05	-4.12E-06	-7.40E-08
8.00E+01	-7.79E-07	4.63E-07	1.36E-05	3.38E-05	-5.66E-06	-1.90E-07
9.00E+01	-7.59E-07	-1.01E-08	1.55E-05	3.84E-05	-5.36E-06	-1.52E-07
1.00E+02	-1.16E-06	-9.49E-07	1.77E-05	4.33E-05	-6.46E-06	6.98E-08
1.50E+02	-1.18E-06	-1.88E-06	2.61E-05	6.44E-05	-9.05E-06	1.49E-06
1.98E+02	-1.71E-07	-1.64E-06	3.50E-05	8.54E-05	-1.22E-05	3.63E-07
2.38E+02	-9.73E-07	-9.33E-07	4.08E-05	1.03E-04	-1.46E-05	1.35E-06
Slope [V/g]	1.80745E-09	-5.8E-09	1.76E-07	4.31E-07	-6.3E-08	8.49E-09

Table of voltages and slopes measured from various pure F_z loads Fig. A4.5

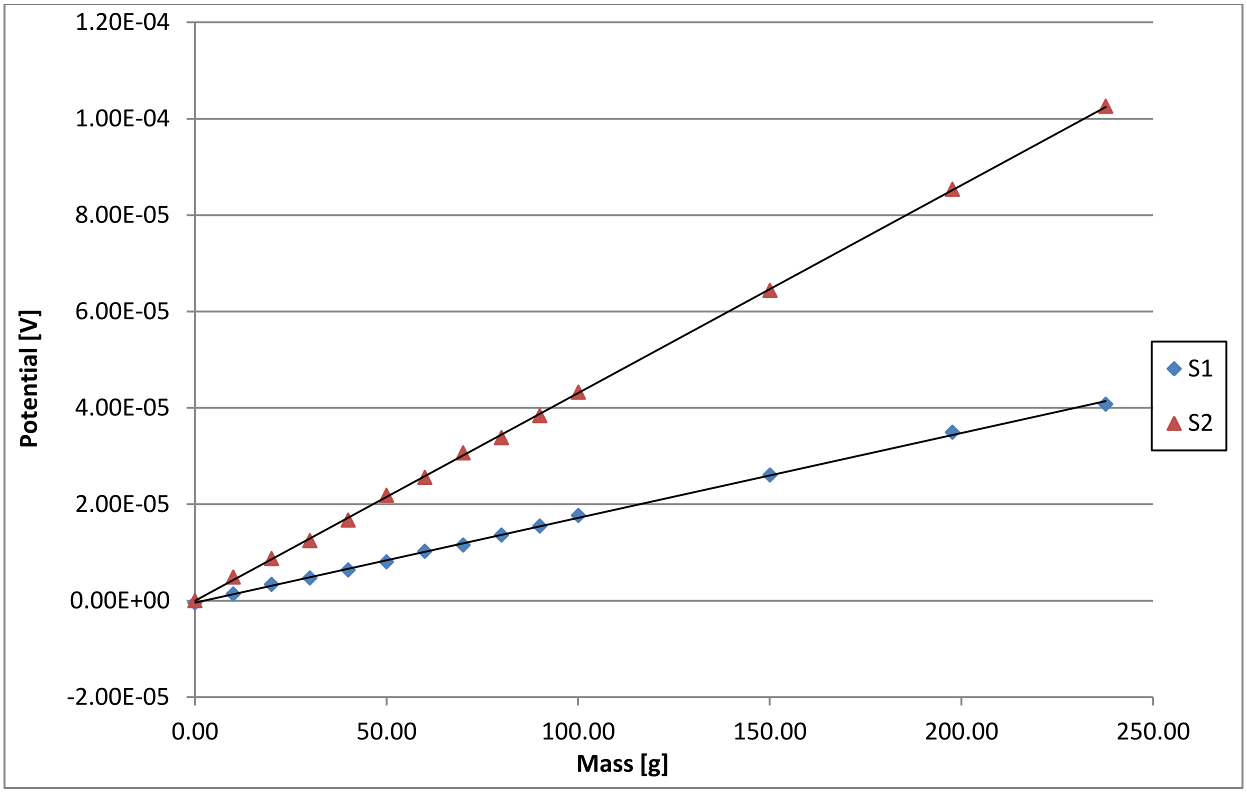

S_1 and S_2 voltages for pure F_z loads Fig. A4.6

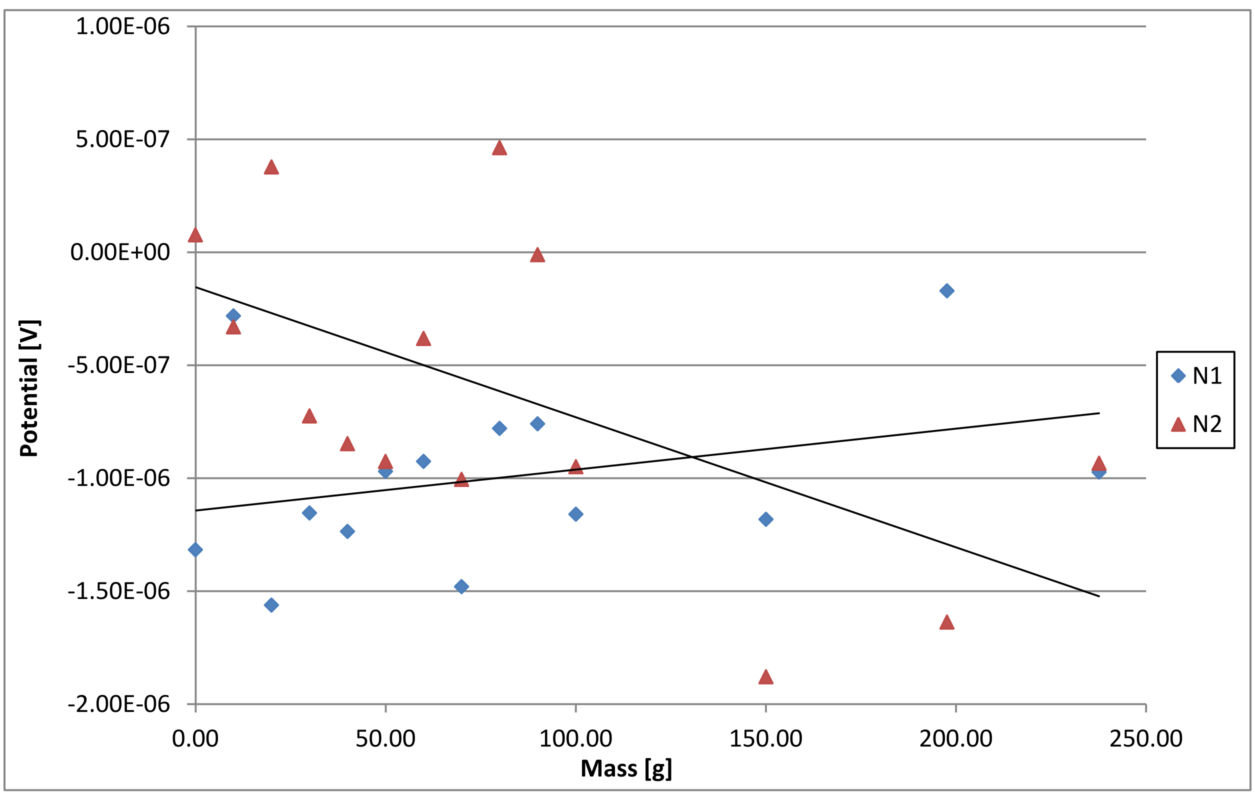

N_1 and N_2 voltages for pure F_z loads Fig. A4.7

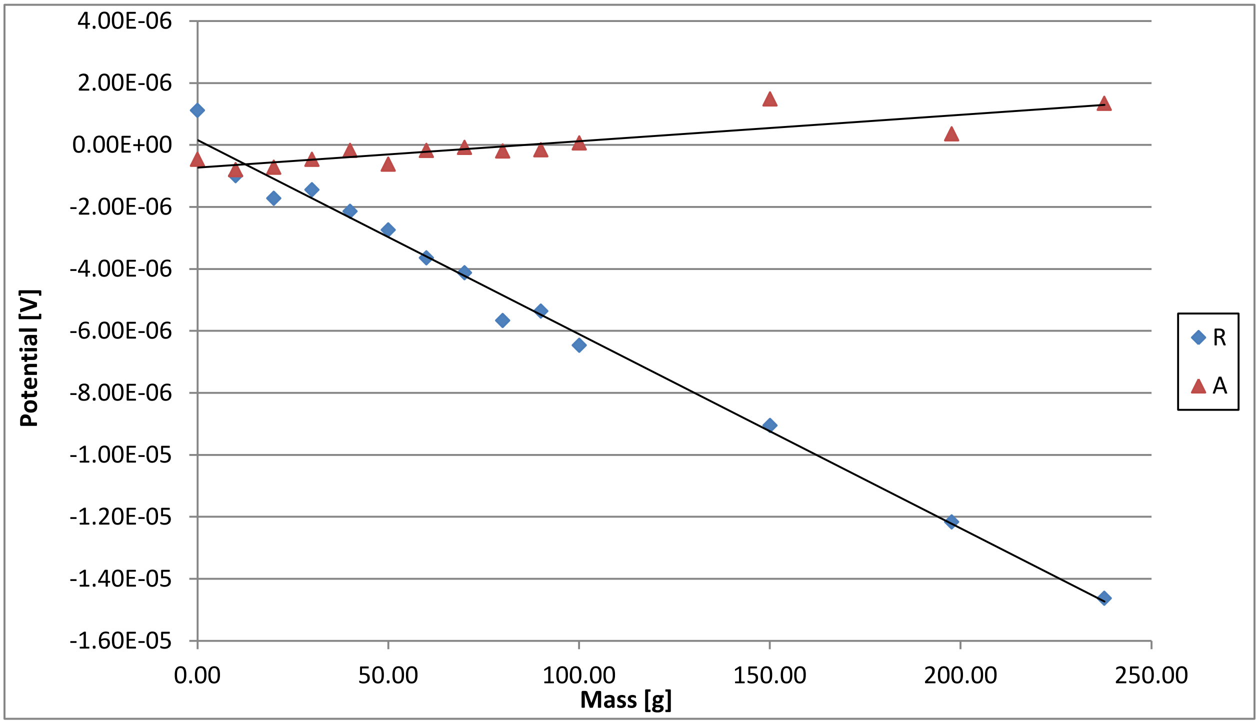

R and A voltages for pure F_z loads Fig. A4.8

F_x data

Mass	N1	N2	S1	S2	R	A
0.00E+00	-4.08E-07	-1.19E-06	-6.17E-07	2.33E-07	-6.67E-07	-4.87E-07
1.00E+01	-5.99E-07	-8.33E-07	-5.83E-07	6.12E-07	6.20E-08	-1.71E-06
2.00E+01	7.63E-08	-6.41E-07	-5.40E-07	6.20E-07	-1.69E-07	-3.36E-06
3.00E+01	-7.07E-07	-8.61E-07	-5.34E-07	2.37E-07	-3.30E-07	-4.43E-06
4.00E+01	-1.25E-08	-7.77E-07	-7.64E-07	2.56E-07	-3.95E-07	-6.04E-06
5.00E+01	-7.77E-07	-2.45E-07	-1.14E-06	-8.41E-08	-6.70E-07	-7.56E-06
6.00E+01	-3.16E-07	-9.01E-08	4.23E-08	5.77E-07	-3.58E-07	-9.42E-06
7.00E+01	-3.48E-07	3.68E-07	-7.49E-07	4.18E-07	-7.94E-07	-1.02E-05
8.00E+01	-1.02E-06	-9.48E-07	-3.66E-07	6.57E-07	1.61E-07	-1.28E-05
9.00E+01	-1.38E-07	-1.36E-06	-9.08E-07	6.28E-07	-2.01E-07	-1.33E-05
1.00E+02	-1.02E-06	-6.91E-07	-1.33E-06	6.82E-07	-3.06E-07	-1.41E-05
1.50E+02	-4.51E-07	-3.98E-07	-8.19E-07	2.23E-07	-1.51E-06	-2.27E-05
1.98E+02	-7.51E-07	-1.09E-06	-8.59E-07	-1.19E-09	4.76E-07	-2.88E-05
2.38E+02	-1.11E-06	-1.32E-06	-1.68E-07	4.30E-07	-2.03E-07	-3.48E-05
Slope [V/g]	-2.6294E-09	-1.7E-09	1.6E-10	-5.7E-10	6.52E-10	-1.4E-07

Table of voltages and slopes for various pure F_x loads Fig. A4.9

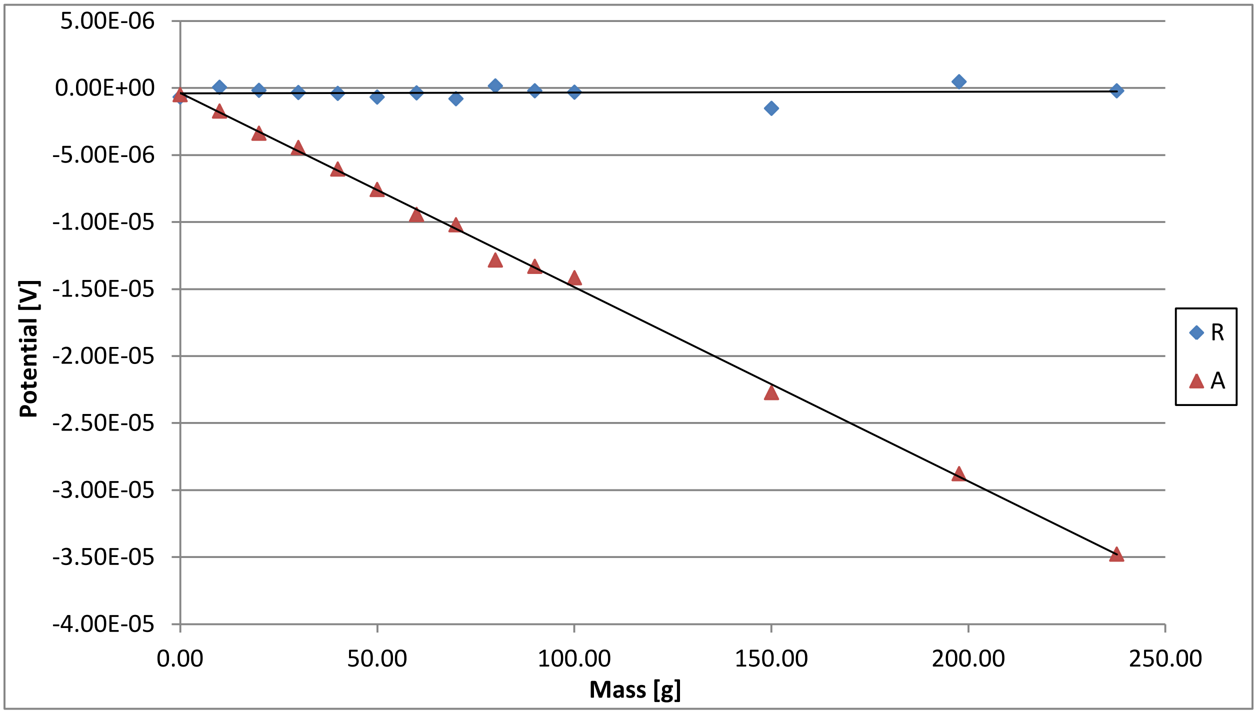

R and A voltages for pure F_x loads Fig. A4.10

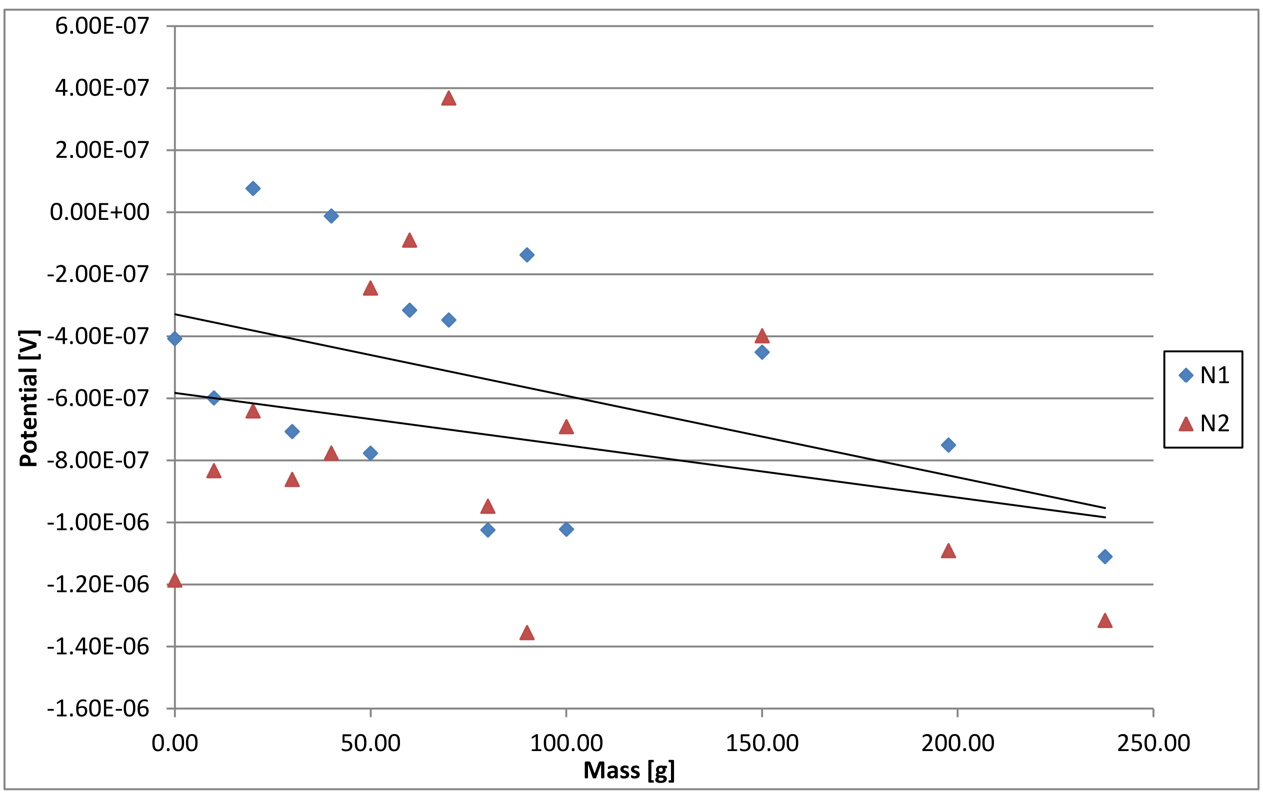

N_1 and N_2 voltages for pure F_x loads Fig. A4.11

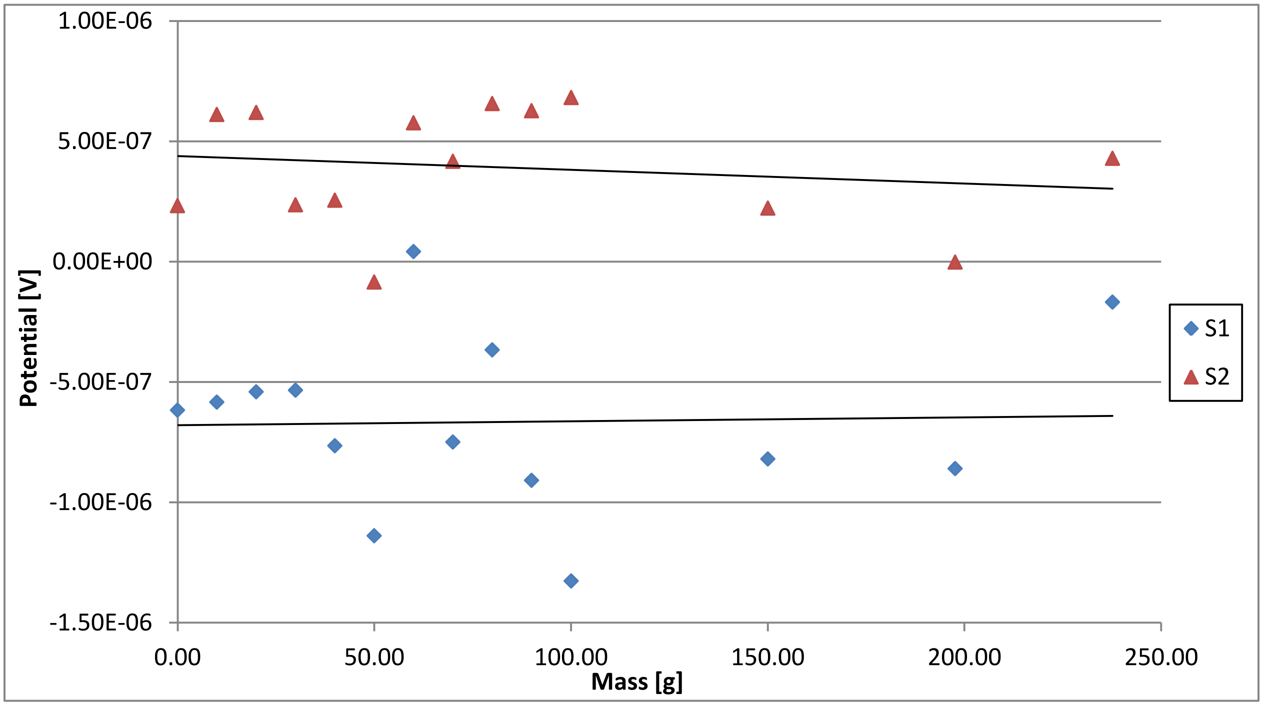

S_1 and S_2 voltages for pure F_x loads Fig. A4.12

M_x data

Mass	N1	N2	S1	S2	R	A
0.00E+00	6.52E-07	7.40E-08	6.51E-07	-2.33E-07	-1.04E-07	-3.46E-08
1.00E+01	6.88E-07	2.66E-07	8.76E-07	2.39E-08	-1.34E-06	-6.78E-07
2.00E+01	2.86E-07	2.39E-08	3.55E-07	4.65E-07	-8.42E-07	3.07E-07
3.00E+01	9.27E-07	4.41E-08	9.90E-08	-2.62E-08	-2.80E-06	-6.20E-07
4.00E+01	8.20E-07	-5.51E-07	7.26E-07	1.81E-07	-3.34E-06	-1.57E-07
5.00E+01	5.27E-07	-2.21E-06	3.44E-07	-3.11E-07	-3.35E-06	1.56E-07
6.00E+01	1.37E-07	-2.41E-06	1.52E-07	5.73E-08	-3.71E-06	-7.58E-08
7.00E+01	9.30E-08	-2.72E-06	2.92E-07	-9.68E-07	-4.76E-06	1.35E-07
8.00E+01	-1.11E-07	-2.47E-06	1.20E-07	-4.19E-07	-6.08E-06	3.30E-07
9.00E+01	5.72E-07	-1.98E-06	3.02E-07	-5.15E-07	-7.60E-06	-1.52E-07
1.00E+02	-2.03E-08	-2.54E-06	7.14E-07	-5.97E-07	-6.45E-06	2.92E-08
1.50E+02	4.12E-07	-2.28E-06	9.67E-07	-1.86E-07	-1.08E-05	9.78E-07
1.98E+02	3.66E-07	-2.01E-06	2.33E-07	7.70E-08	-1.43E-05	9.63E-07
2.38E+02	2.56E-07	-1.58E-06	2.49E-07	-4.32E-07	-1.71E-05	1.51E-06
Slope [V/g]	-1.62249E-09	-8.7E-09	-6.2E-10	-1.3E-09	-7.1E-08	7.45E-09

Voltages and slopes of pure M_x load Fig. A4.13

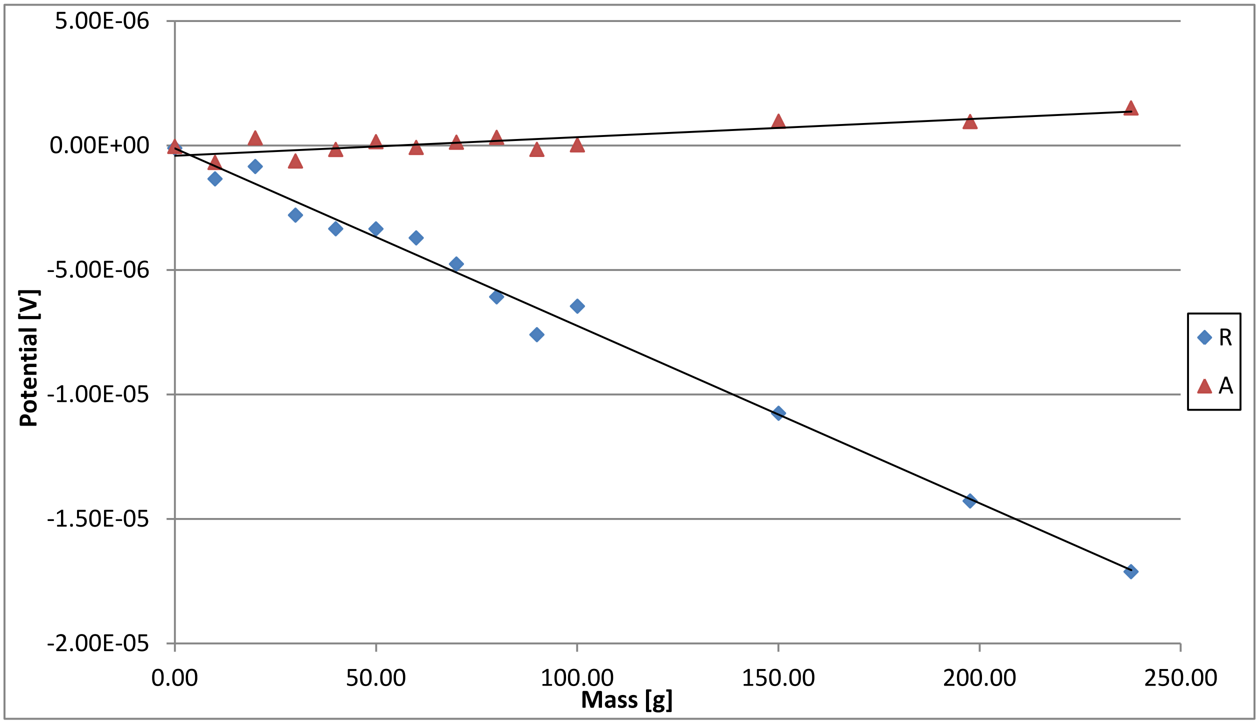

R and A voltages for pure M_x load Fig. A4.14

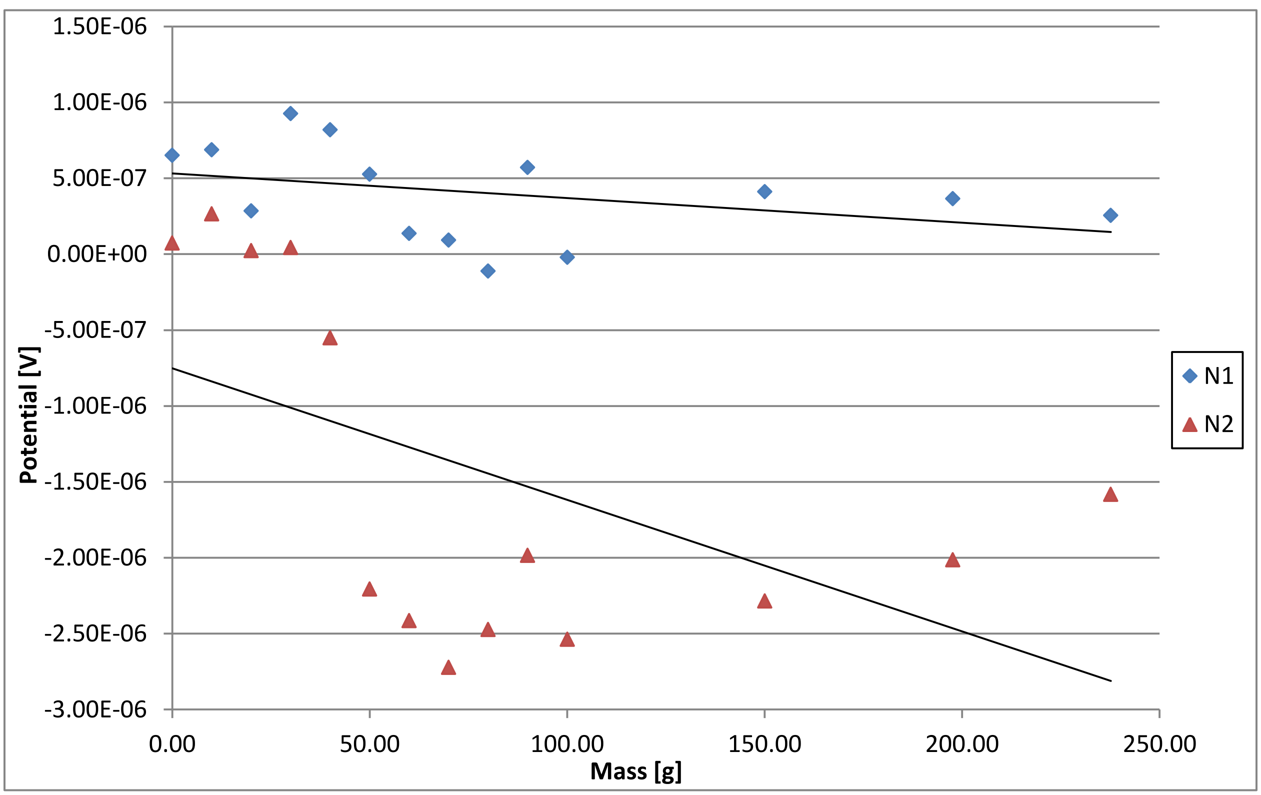

N_1 and N_2 voltages for pure M_x loads Fig. A4.15

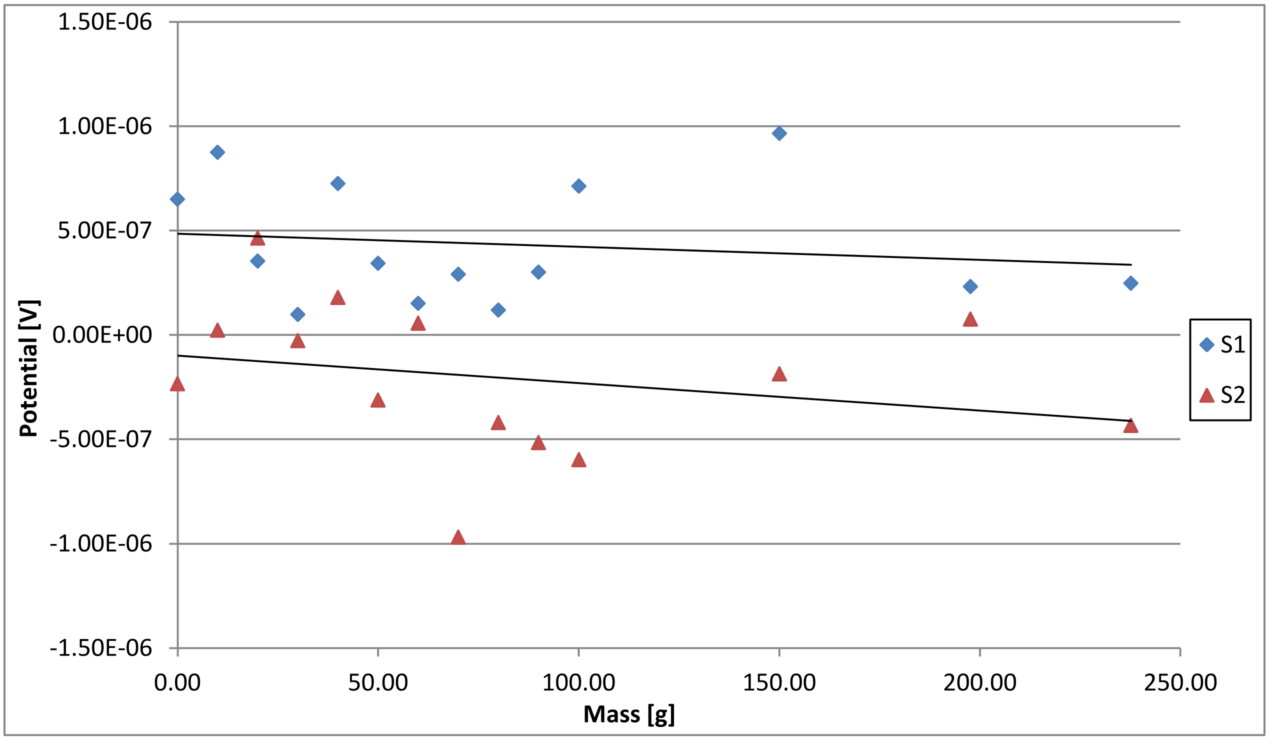

S_1 and S_2 voltages for pure M_x loads Fig A4.16

M_y data

Mass [g] (3.81cm arm)	N1 [V]	N2[V]	S1 [V]	S2 [V]	R [V]	A [V]
20	1.97E-06	-5.39E-07	-8.05E-06	-1.82E-05	2.43E-06	2.65E-07
100.07	1.43E-06	1.30E-06	-3.89E-05	-9.01E-05	1.39E-05	-3.03E-07
197.68	8.96E-07	1.50E-06	-6.90E-05	-1.60E-04	2.41E-05	-2.30E-06
Slope [V/g]	-6.01182E-09	1.11E-08	-3.4E-07	-8E-07	1.21E-07	-1.5E-08
Slope [V/Nm]	-0.00015779	0.000292	-0.00896	-0.02088	0.003183	-0.00039
Mass [g] (5.08cm arm)	N1 [V]	N2[V]	S1 [V]	S2 [V]	R [V]	A [V]
20	1.92E-06	-5.60E-07	-1.09E-05	-2.10E-05	4.33E-06	1.02E-06
100.07	1.84E-06	1.27E-06	-4.74E-05	-9.85E-05	1.49E-05	-1.13E-06
197.68	1.47E-06	6.47E-07	-8.98E-05	-1.91E-04	2.84E-05	-1.99E-06
Slope [V/g]	-2.58332E-09	6.32E-09	-4.4E-07	-9.6E-07	1.35E-07	-1.7E-08
Slope [V/Nm]	-5.08528E-05	0.000166	-0.01165	-0.02518	0.003556	-0.00044
Mass [g] (6.35cm arm)	N1 [V]	N2[V]	S1 [V]	S2 [V]	R [V]	A [V]
20	1.91E-06	-2.51E-07	-1.22E-05	-2.33E-05	4.02E-06	5.63E-07
100.07	1.42E-06	1.55E-06	-5.56E-05	-1.09E-04	1.71E-05	-6.94E-07
197.68	1.21E-06	2.29E-06	-1.06E-04	-2.09E-04	3.17E-05	-2.69E-06
Slope [V/g]	-3.89556E-09	1.41E-08	-5.3E-07	-1E-06	1.56E-07	-1.8E-08
Slope [V/Nm]	-6.13474E-05	0.000369	-0.01388	-0.02749	0.004088	-0.00048
Mass [g] (7.62cm arm)	N1 [V]	N2[V]	S1 [V]	S2 [V]	R [V]	A [V]
20	2.25E-06	-3.94E-07	-1.57E-05	-2.57E-05	4.07E-06	3.00E-07
100.07	1.69E-06	7.75E-07	-6.40E-05	-1.18E-04	1.91E-05	-7.50E-07
197.68	1.61E-06	2.03E-06	-1.22E-04	-2.26E-04	3.51E-05	-2.37E-06
Slope [V/g]	-3.50267E-09	1.36E-08	-6E-07	-1.1E-06	1.74E-07	-1.5E-08
Slope [V/Nm]	-4.59668E-05	0.000357	-0.01576	-0.0296	0.004579	-0.0004
Mass [g] (8.89cm arm)	N1 [V]	N2[V]	S1 [V]	S2 [V]	R [V]	A [V]
20	1.61E-06	6.58E-07	-1.81E-05	-2.89E-05	5.22E-06	8.93E-07
100.07	1.69E-06	1.20E-06	-7.27E-05	-1.27E-04	2.04E-05	-4.55E-07
197.68	1.38E-06	2.68E-06	-1.39E-04	-2.43E-04	3.71E-05	-2.68E-06
Slope [V/g]	-1.35807E-09	1.15E-08	-6.8E-07	-1.2E-06	1.79E-07	-2E-08
Slope [V/Nm]	-1.52764E-05	0.000302	-0.0178	-0.03169	0.004698	-0.00053
Average Slopes [V/Nm]	-6.62468E-05	0.000297	-0.01361	-0.02697	0.004021	-0.00045

Voltages and slopes for various M_y loads Fig. A4.16

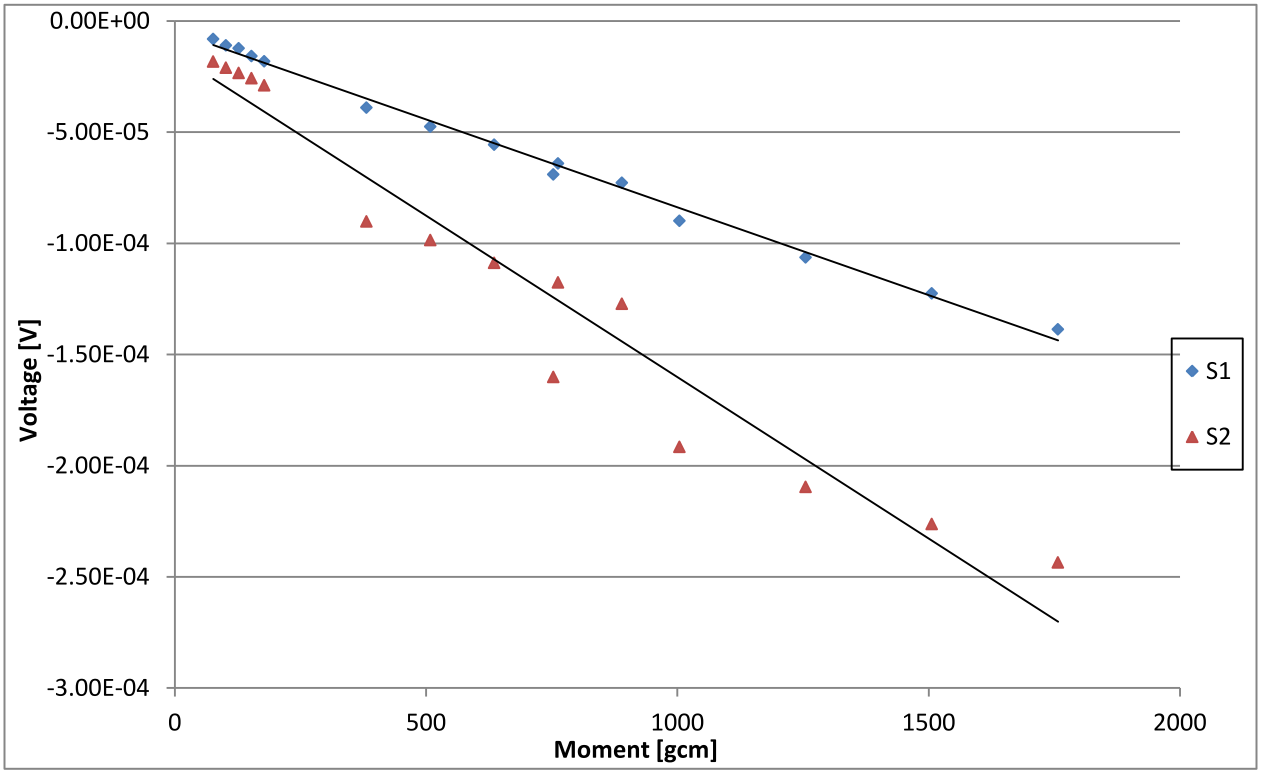

S_1 and S_2 voltages for M_y loads Fig. A4.17

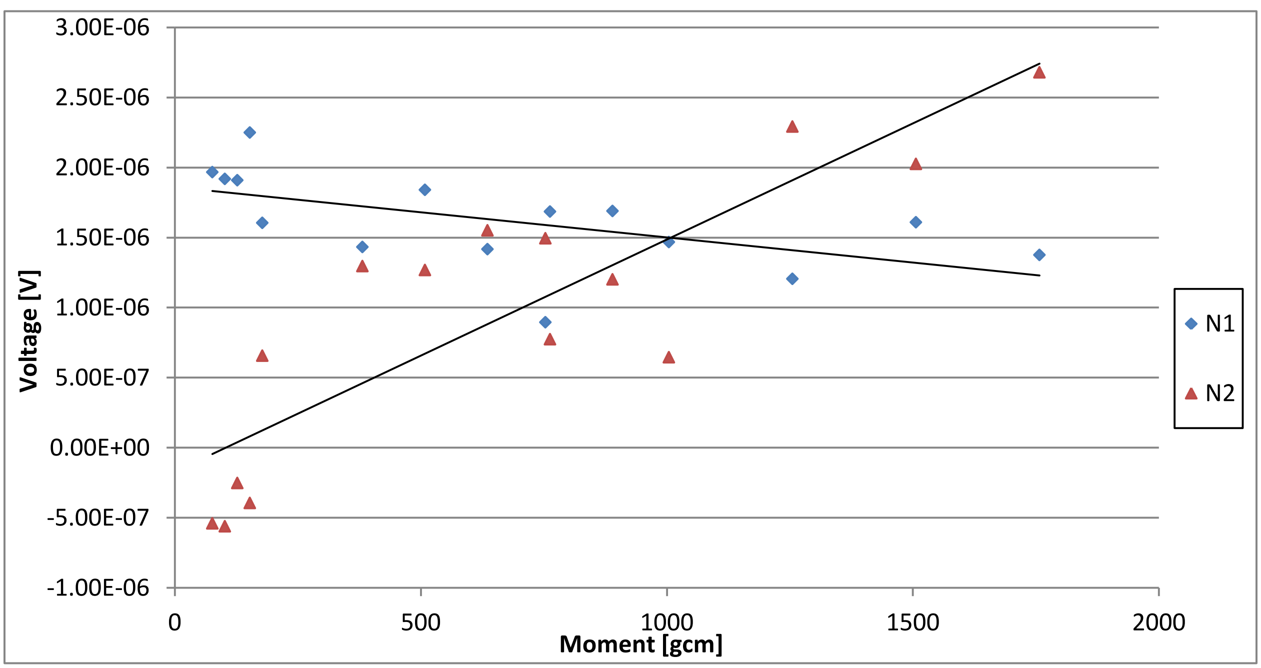

N_1 and N_2 voltages for M_y loads Fig. A4.18

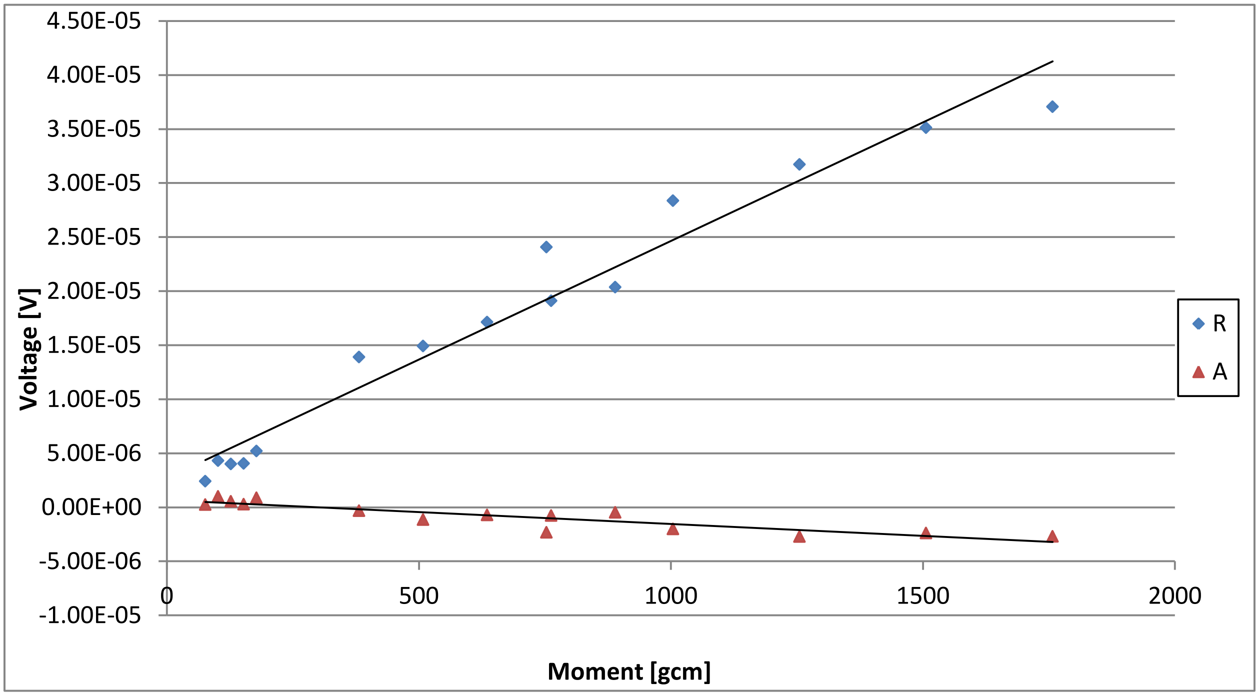

R and A voltages for M_y loads Fig. A4.19

M_z data

Mass [g]	N1 [V]	N2[V]	S1 [V]	S2 [V]	R [V]	A [V]
20	-2.14E-06	-1.23E-06	-1.33E-07	2.78E-07	-6.67E-07	4.69E-07
100.07	-3.46E-06	-5.19E-06	-8.01E-07	3.03E-07	1.25E-06	-1.61E-07
197.68	-6.50E-06	-9.04E-06	7.07E-07	-4.67E-07	4.82E-08	-5.90E-07
Slope [V/g]	-2.5E-08	-4.4E-08	5.11E-09	-4.3E-09	3.43E-09	-5.9E-09
Slope [V/Nm]	-0.00065	-0.00115	0.000134	-0.00011	9.02E-05	-0.00015
Mass [g]	N1 [V]	N2[V]	S1 [V]	S2 [V]	R [V]	A [V]
20	-3.08E-06	-3.59E-06	-6.00E-07	4.65E-07	-1.02E-07	4.85E-07
100.07	-1.11E-05	-1.29E-05	-2.47E-07	1.19E-07	1.30E-06	-7.31E-07
197.68	-2.01E-05	-2.37E-05	-1.29E-07	-4.70E-07	5.57E-07	-2.46E-06
Slope [V/g]	-9.6E-08	-1.1E-07	2.6E-09	-5.3E-09	3.3E-09	-1.7E-08
Slope [V/Nm]	-0.00189	-0.00297	6.82E-05	-0.00014	8.66E-05	-0.00044
Mass [g]	N1 [V]	N2[V]	S1 [V]	S2 [V]	R [V]	A [V]
20	-5.88E-06	-5.48E-06	-4.64E-07	2.88E-07	5.19E-07	1.64E-07
100.07	-1.79E-05	-2.08E-05	-1.33E-07	4.78E-07	1.38E-06	-1.48E-06
197.68	-3.45E-05	-3.87E-05	-1.37E-08	-7.87E-07	1.73E-06	-4.65E-06
Slope [V/g]	-1.6E-07	-1.9E-07	2.49E-09	-6.3E-09	6.71E-09	-2.7E-08
Slope [V/Nm]	-0.00254	-0.0049	6.53E-05	-0.00017	0.000176	-0.00072
Mass [g]	N1 [V]	N2[V]	S1 [V]	S2 [V]	R [V]	A [V]
20	-9.17E-06	-8.21E-06	-8.13E-09	9.35E-08	3.62E-07	-5.81E-07
100.07	-2.55E-05	-2.79E-05	-7.60E-07	5.79E-07	2.25E-06	-3.09E-06
197.68	-4.77E-05	-5.26E-05	-1.55E-06	-7.30E-07	2.83E-06	-5.71E-06
Slope [V/g]	-2.2E-07	-2.5E-07	-8.7E-09	-5E-09	1.36E-08	-2.9E-08
Slope [V/Nm]	-0.00285	-0.00655	-0.00023	-0.00013	0.000357	-0.00075
Mass [g]	N1 [V]	N2[V]	S1 [V]	S2 [V]	R [V]	A [V]
20	-1.10E-05	-1.06E-05	3.57E-07	-4.65E-07	-2.41E-08	-2.36E-07
100.07	-3.34E-05	-3.56E-05	-1.26E-06	4.79E-07	2.30E-06	-4.69E-06
197.68	-6.24E-05	-6.66E-05	-9.81E-07	-8.67E-07	3.01E-06	-7.66E-06
Slope [V/g]	-2.9E-07	-3.2E-07	-7.2E-09	-2.7E-09	1.67E-08	-4.1E-08
Slope [V/Nm]	-0.00326	-0.00828	-0.00019	-7E-05	0.000439	-0.00109
Average Slope [V/Nm]	-0.00224	-0.00477	-3E-05	-0.00012	0.00023	-0.00063

Voltages and slopes for various M_z loads Fig. A4.20

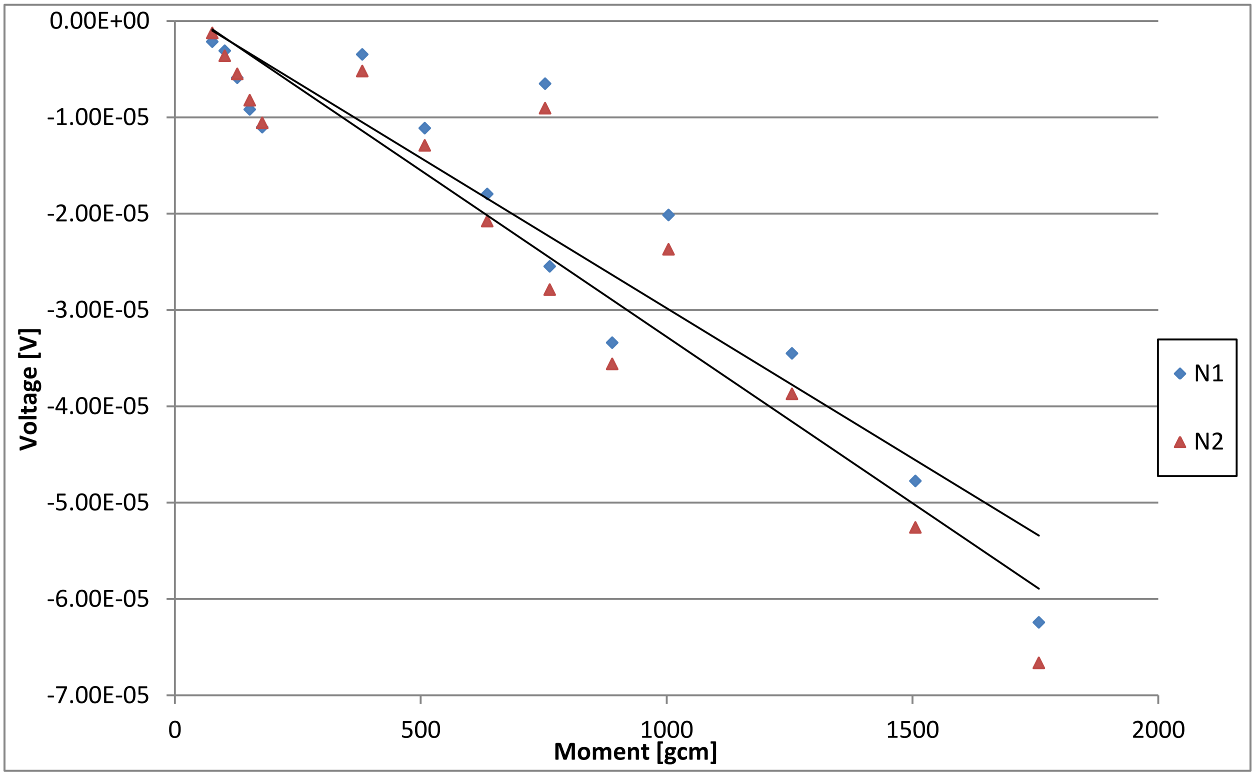

N_1 and N_2 voltages for M_z loads Fig. A4.21

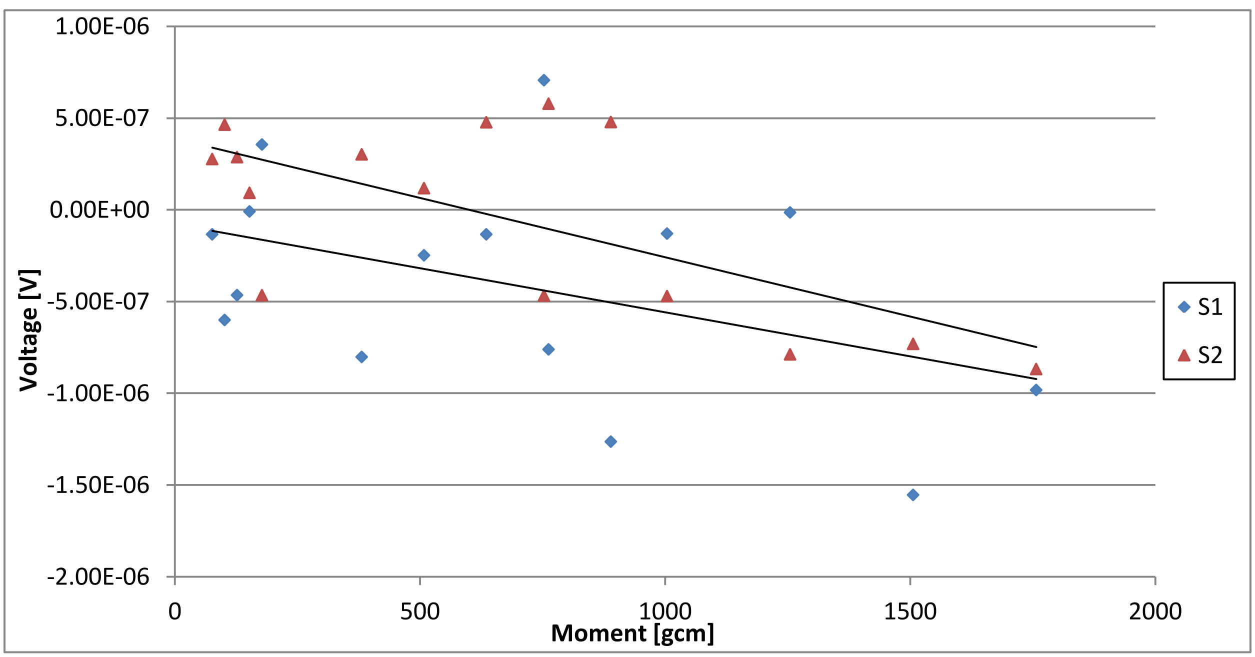

S_1 and S_2 voltages for M_z loads Fig. A4.22

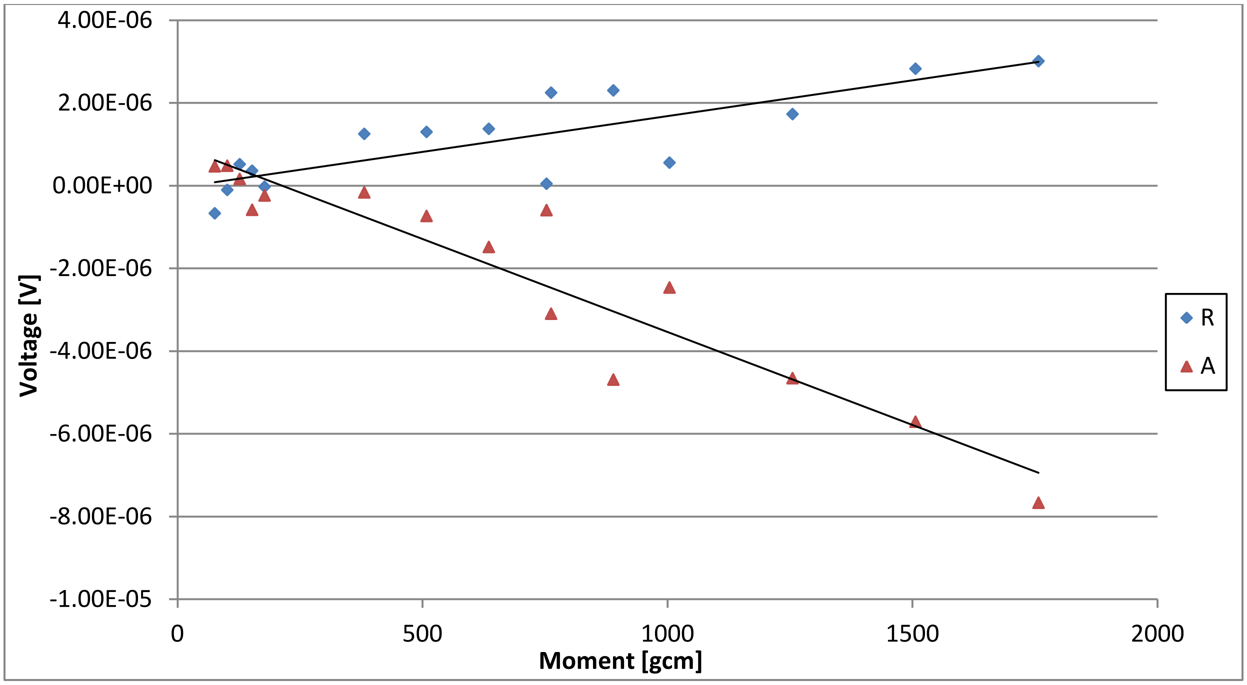

R and A voltages for M_z loads Fig. A4.23

References

[1] (Technovelgy LLC, Technovelgy.com, 2005), Vol. 2013.

[2] UAS Vision, 2011), Vol. 2013.

[3] Aerolab, (Aerolab, Aerolab, 2002).

[4] J. B. Barlow, W. H. J. Rae, and A. Pope, *Low Speed Wind Tunnel Testing* (John Wiley & Sons, Inc., Canada, 1999).

[5] T. Carpenter, 2011).

[6] T. Carpenter, 2011).

[7] P. Carter, esotc.org, 1998), Vol. 2013.

[8] Deltabrown, Wikipedia, 2007), Vol. 2013, p. CAD model of an internal force and moment balance.

[9] B. F. R. Ewald, Measurement Science & Technology **11**, R81 (2000).

[10] R. S. Figliola and D. E. Beasley, *Theory and Design for Mechanical Measurements* (John Wiley and Sons, 2010).

[11] J. M. Grasmeyer and K. M. T., American Institute for Aeronautics and Astronautics (2001).

[12] thomas, Revista Aerea, 2008), Vol. 2013.

Acknowledgements

The vast majority of the programming was accomplished or overseen by Trenton Carpenter. Many thanks go to Mr. Carpenter for his well written and extensive programs and his help with the project.

The author would also like to thank Dr. Roberto Albertani of the Advanced Mechanics and Composites Technology lab for his continued support and insight into this project.